Active Fault-Tolerant Incremental Sliding-Mode Flight Control Against Control Reversal

Chang, Jing; De Breuker, Roeland; Wang, Xuerui

DOI
10.2514/1.G006690

Publication date
2022

Document Version
Final published version

Published in
Journal of Guidance, Control, and Dynamics

JOURNAL OF GUIDANCE, CONTROL, AND DYNAMICS
Vol. 45, No. 12, December 2022

Engineering Notes

Active Fault-Tolerant Incremental Sliding-Mode Flight Control Against Control Reversal

Jing Chang*
Xidian University, 710126 Xi'an, People's Republic of China
and
Roeland De Breuker† and Xuerui Wang‡
Delft University of Technology, 2629 HS Delft, The Netherlands

https://doi.org/10.2514/1.G006690

I. Introduction

AIRCRAFT safety is threatened by various in-flight faults. One of the critical fault cases is control reversal, which indicates the phenomenon that the real control effect is reversed from what is expected [1]. Control reversal can be caused by various factors, including aeroelasticity [2], hardware connection errors [3], pilot errors [4], and coupling effects [5]. When an aircraft wing has insufficient torsional stiffness, the trailing-edge aileron deflection can change the local angle of attack of the wing, consequently leading to aeroelasticity-caused roll reversal. This is often coupled with high-speed effects such as compressibility. Hardware connection errors in the hydraulic actuation system can also lead to control reversal. Faulty actuators were the cause of several rudder reversals on Boeing 737 aircraft in the 1990s, contributing to accidents [3].

Control reversal can easily lead to the loss of control in-flight [1]. Unfortunately, it is a challenging problem that many flight control methods, such as model reference adaptive control [6] and sliding mode control [7], cannot deal with. Almost all the nonlinear robust control designs using Lyapunov's direct methods require the control direction information, which is used to determine the signs of the time derivative of the corresponding Lyapunov functions [1,6,8,9]. Controllers using the Lyapunov argument are much more difficult to design if a priori knowledge of control directions is unavailable. In the mathematics and control communities, the challenging unknown control direction problem has been solved by introducing the Nussbaum gain in the adaptive control design [8,10]. This approach has wide applicability in various mechanical systems [10,11]. However, the Nussbaum-gain-based control often requires very high control frequency. More importantly, it only has guaranteed stability when the control sign is unknown but invariant. Therefore, it cannot deal with in-flight control reversal. Another solution is the fault-tolerant control (FTC) framework [12], which has great potential to achieve aircraft flight control tasks even in the presence of faults.

The FTC schemes can be classified into passive FTC and active FTC. The passive FTC approach is only robust against prespecified faults, excluding control reversal. By contrast, the active approach generally has border applicability because its control law is aware of faults [12,13]. The fault information can be disclosed by online fault detection and identification (FDI) or fault estimation (FE), which adopts methods such as unknown input observer [14], sliding mode observer [15], Kalman filter [16], and learning observer [17]. Although many FDI/FE methods for aircraft sensory and actuator faults have been proposed, managing simultaneously occurring multisource faults is still an open challenge. Moreover, some practical factors including external disturbances, sensing bias and noise, and model uncertainties can seriously reduce the performance of the existing FDI/FE methods [15]. Furthermore, to reconstruct the accurate fault information, state-of-the-art FDI/FE observers often require a strict matching condition or a strictly positive-real condition [18], which can be violated when there are redundant and strongly coupled sensors and/or actuators.

Once the fault information is disclosed, another important part of active FTC is the control design. A multiple-model adaptive control scheme was developed in [19] to compensate for actuation sign errors and inertia parameter uncertainties in a rigid spacecraft attitude tracking control problem. It uses a control switching algorithm based on a set of adaptive estimators to guarantee the global attitude tracking performance, in which 2^p estimators and 2^q cost functions are required for a p-input, q-output system. This control strategy was also extended for a flexible spacecraft tracking problem in the presence of actuation sign faults and aeroelastic uncertainties in [20]. Recently, one inverse gain switching adaptive control method was proposed in [1] for tolerating control reversal and parametric uncertainties. This challenging control problem was solved by finding the fixed point solution for a model reference adaptive control with the dynamic inverse. However, it can only deal with linear systems and potentially suffers from Zeno behavior.

Nonlinear incremental control has shown great potential in solving aircraft FTC problems [21,22]. The most well-known incremental control method is incremental nonlinear dynamic inversion (INDI) [22,23]. The only model information required by INDI is the control effectiveness estimation. Even so, by exploiting sensory measurements, the robustness of INDI against model uncertainties and external disturbances is significantly improved over that of nonlinear dynamic inversion [23]. Incremental sliding mode control (INDI-SMC) is a hybridization between INDI and (higher-order) sliding-mode controllers/observers for generic multi-input–multi-output (MIMO) nonlinear systems [21]. Lyapunov-based analysis and simulation validations show that INDI-SMC can passively resist a wider range of uncertainties, actuator faults, and structural damage with reduced minimum possible control/observer gains [21].

Despite the promising robustness of INDI-SMC, it requires one critical sufficient condition: the estimation of the control effectiveness matrix should be sufficiently close to its true value (quantitative expression can be found in [21]). However, in the control reversal fault case, this condition is violated. Consequently, neither the boundedness of the residual error nor the stability of the closed-loop system can be guaranteed. Moreover, the Lyapunov-based stability and robustness analysis of INDI-SMC also has limitations. First, sensing errors, especially that of the high-order output derivatives, are not considered. Second, the assumption of sufficiently high sampling frequency is applied without presenting an explicit criterion for how high the sampling frequency should be.

Received 17 January 2022; revision received 25 June 2022; accepted for publication 1 September 2022; published online 14 October 2022.

*Assistant Professor, School of Aerospace Science and Technology; also Visiting Scholar, Faculty of Aerospace Engineering, Delft University of Technology, 2629 HS Delft, The Netherlands; jchang@xidian.edu.cn, j.chang-2@tudelft.nl. Member AIAA.

†Associate Professor, Faculty of Aerospace Engineering, Kluyverweg 1; r.debreuker@tudelft.nl. Associate Fellow AIAA.

‡Assistant Professor, Faculty of Aerospace Engineering, Kluyverweg 1; x.wang-6@tudelft.nl. Member AIAA.

This Note proposes an active incremental sliding mode control approach denoted as A-INDI-SMC. It is empowered with an online incremental FDI unit, which can promptly reconstruct control sign changes despite multisource faults, sensing bias and noise, and model uncertainties. The harmful Zeno behavior is also prevented by using multiple time-step incremental measurements and the dwell-time technique. Moreover, sensing errors are considered in the Lyapunov-based stability and robustness analysis. Furthermore, an explicit and quantifiable expression for the ultimate bound of the tracking error, as a function of the sampling frequency and perturbation bounds, is derived. The effectiveness of A-INDI-SMC is validated by an aircraft command tracking problem, in the presence of control reversal, model uncertainties, sensing errors, actuator faults, and structural damage.

The rest of this Note is structured as follows. The INDI-SMC method is analyzed in Sec. II. Section III proposes the A-INDI-SMC. The aircraft FTC validations are presented in Sec. IV. Conclusions are drawn in Sec. V.

II. Analysis and Limitation Exposure of the Incremental Sliding Mode Control

This section briefly reviews the incremental sliding mode control method and its corresponding stability analysis. Furthermore, the limitations of INDI-SMC, especially in the presence of control reversal, are exposed.

A. System Dynamics and Control Objective

Consider an MIMO nonlinear system described in the continuous time domain by

$$\dot{\boldsymbol{x}} = \boldsymbol{f}(\boldsymbol{x},\boldsymbol{u}), \quad \boldsymbol{y} = \boldsymbol{h}(\boldsymbol{x}) \tag{1}$$

where $\boldsymbol{x} \in \mathbb{R}^n$, $\boldsymbol{u} \in \mathbb{R}^m$, and $\boldsymbol{y} \in \mathbb{R}^m$ are the system state, input, and output, respectively, and $\boldsymbol{f}:\mathbb{R}^n \to \mathbb{R}^n$ and $\boldsymbol{h}:\mathbb{R}^n \to \mathbb{R}^m$ are continuous functions. The elements of $\boldsymbol{h}$ are denoted as h_i, $i = 1,\ldots,m$. Using the Lie derivatives, the input–output mapping of the system is given by

$$\boldsymbol{y}^{(\boldsymbol{\rho})} = \boldsymbol{g}(\boldsymbol{x},\boldsymbol{u}) \tag{2}$$

where $\boldsymbol{\rho} = [\rho_1,\rho_2,\ldots,\rho_m]^\top$ represents the relative degree, and $\boldsymbol{g}(\boldsymbol{x},\boldsymbol{u}) = [\mathcal{L}_f^{\rho_1}h_1, \mathcal{L}_f^{\rho_2}h_2,\ldots,\mathcal{L}_f^{\rho_m}h_m]^\top$. Define the external state as $\boldsymbol{\xi}^\top = [\boldsymbol{\xi}_1^\top,\boldsymbol{\xi}_2^\top,\ldots,\boldsymbol{\xi}_m^\top]$, $\boldsymbol{\xi}_i = [h_i,\mathcal{L}_f h_i,\ldots,\mathcal{L}_f^{(\rho_i-1)}h_i]^\top$, $i = 1,\ldots,m$. Denote $n_e = \rho_1+\rho_2+\cdots+\rho_m$, then the internal state vector is $\boldsymbol{\eta} \in \mathbb{R}^{n-n_e}$. Apply the change of coordinates as $\boldsymbol{z} \mapsto T(\boldsymbol{x})$, which is a diffeomorphism on a domain D, then a new state representation $\boldsymbol{z}^\top = [\boldsymbol{\eta}^\top,\boldsymbol{\xi}^\top]$ is created. The nonlinear system in Eq. (1) is then transformed into a canonical form as [23]

$$\dot{\boldsymbol{\eta}} = \boldsymbol{f}_{\text{in}}(\boldsymbol{\eta},\boldsymbol{\xi}), \quad \dot{\boldsymbol{\xi}} = \boldsymbol{A}_c\boldsymbol{\xi} + \boldsymbol{B}_c\boldsymbol{g}(\boldsymbol{x},\boldsymbol{u}), \quad \boldsymbol{y} = \boldsymbol{C}_c\boldsymbol{\xi} \tag{3}$$

Taking the first-order Taylor series expansion of Eq. (2) at $t-h$, where t is the current time and h is one sampling interval, we obtain the incremental dynamics:

$$\begin{aligned}\boldsymbol{y}^{(\boldsymbol{\rho})} &= \boldsymbol{y}^{(\boldsymbol{\rho})}\Big|_0 + \frac{\partial \boldsymbol{g}(\boldsymbol{x},\boldsymbol{u})}{\partial \boldsymbol{x}}\Big|_0 \Delta\boldsymbol{x} + \frac{\partial \boldsymbol{g}(\boldsymbol{x},\boldsymbol{u})}{\partial \boldsymbol{u}}\Big|_0 \Delta\boldsymbol{u} + \boldsymbol{R}_1(\boldsymbol{x},\boldsymbol{u},h)\\ &\triangleq \boldsymbol{y}_0^{(\boldsymbol{\rho})} + \mathcal{A}_0(\boldsymbol{x})\Delta\boldsymbol{x} + \boldsymbol{\mathcal{B}}_0(\boldsymbol{x})\Delta\boldsymbol{u} + \boldsymbol{R}_1(\boldsymbol{x},\boldsymbol{u},h)\end{aligned} \tag{4}$$

where $(\cdot)|_0$ means evaluating $(\cdot)$ at $(\boldsymbol{x}_0 = \boldsymbol{x}(t-h), \boldsymbol{u}_0 = \boldsymbol{u}(t-h), \boldsymbol{d}_0 = \boldsymbol{d}(t-h))$. The state and control variations in one incremental time step are $\Delta\boldsymbol{x} = \boldsymbol{x}-\boldsymbol{x}_0$ and $\Delta\boldsymbol{u} = \boldsymbol{u}-\boldsymbol{u}_0$, respectively. $\boldsymbol{R}_1$ is the expansion remainder, whose Lagrange form is

$$\begin{aligned}\boldsymbol{R}_1(\boldsymbol{x},\boldsymbol{u},h) = \frac{1}{2}\frac{\partial^2 \boldsymbol{g}(\boldsymbol{x},\boldsymbol{u})}{\partial \boldsymbol{x}^2}\Big|_m \Delta\boldsymbol{x}^2 + \frac{1}{2}\frac{\partial^2 \boldsymbol{g}(\boldsymbol{x},\boldsymbol{u})}{\partial \boldsymbol{u}^2}\Big|_m \Delta\boldsymbol{u}^2\\ + \frac{\partial^2 \boldsymbol{g}(\boldsymbol{x},\boldsymbol{u})}{\partial \boldsymbol{x}\partial \boldsymbol{u}}\Big|_m \Delta\boldsymbol{x}\Delta\boldsymbol{u}\end{aligned} \tag{5}$$

where $(\cdot)|_m$ means evaluating $(\cdot)$ at $(\boldsymbol{x}_m,\boldsymbol{u}_m)$, where $\boldsymbol{x}_m \in [\boldsymbol{x}(t-h),\boldsymbol{x}(t)]$ and $\boldsymbol{u}_m \in [\boldsymbol{u}(t-h),\boldsymbol{u}(t)]$.

Assumption 1: Assume that the reference signal $\boldsymbol{y}_r = [y_{r,1}, y_{r,2},\ldots,y_{r,m}]^\top$ and its derivatives up to $y_{r,i}^{(\rho_i)}$ are bounded and continuous.

Because of the limited actuator bandwidth, not all the reference commands (such as the step reference) can be perfectly tracked in reality. In practice, the sharp commands are commonly smoothened using command filtering, after implementing which, Assumption 1 is normally satisfied [15,23].

Denote the reference state vector as $\boldsymbol{r} = [\boldsymbol{r}_1,\boldsymbol{r}_2,\ldots,\boldsymbol{r}_m]^\top$ with $\boldsymbol{r}_i = [y_{r,i}, y_{r,i}^{(1)},\ldots,y_{r,i}^{(\rho_i-1)}]$, $i = 1,\ldots,m$. Define the tracking error vector as $\boldsymbol{e} = \boldsymbol{\xi}-\boldsymbol{r}$. Substitute Eq. (4) into Eq. (3), then the error dynamics are given by

$$\dot{\boldsymbol{e}} = \boldsymbol{A}_c\boldsymbol{e} + \boldsymbol{B}_c\Big[\boldsymbol{y}_0^{(\boldsymbol{\rho})} + \boldsymbol{\mathcal{B}}_0(\boldsymbol{x})\Delta\boldsymbol{u} + \mathcal{A}_0(\boldsymbol{x})\Delta\boldsymbol{x} + \boldsymbol{R}_1(\boldsymbol{x},\boldsymbol{u},h) - \boldsymbol{y}_r^{(\boldsymbol{\rho})}\Big] \tag{6}$$

where $\boldsymbol{y}_r^{(\boldsymbol{\rho})} = [y_{r,1}^{\rho_1}, y_{r,2}^{\rho_2},\ldots,y_{r,m}^{\rho_m}]^\top$. The control objective is to make $\boldsymbol{y}$ tracks its reference $\boldsymbol{y}_r$ while tolerating faults.

Considering model uncertainties, actuator faults, structural damage, and control reversal, the control effectiveness matrix of a system is modeled as $\boldsymbol{\mathcal{B}}_0(\boldsymbol{x}) = (\hat{\boldsymbol{\mathcal{B}}}_0(\boldsymbol{x}) + \tilde{\boldsymbol{\mathcal{B}}}_0(\boldsymbol{x}))\boldsymbol{\Lambda}$, where $\hat{\boldsymbol{\mathcal{B}}}_0(\boldsymbol{x})$ is a *known* nominal model [20,24]; $\tilde{\boldsymbol{\mathcal{B}}}_0(\boldsymbol{x})$ represents the *unknown* control distribution matrix uncertainty owing to actuator faults and structural damage; $\boldsymbol{\Lambda} = \text{diag}\{w_1, w_2, \ldots, w_m\}$, $|w_i| = 1$, $i = 1,\ldots m$, is an *unknown* time-varying sign-switching matrix. Consequently, the incremental input–output mapping in Eq. (4) is written as

$$\boldsymbol{y}^{(\boldsymbol{\rho})} = \boldsymbol{y}_0^{(\boldsymbol{\rho})} + (\hat{\boldsymbol{\mathcal{B}}}_0(\boldsymbol{x}) + \tilde{\boldsymbol{\mathcal{B}}}_0(\boldsymbol{x}))\boldsymbol{\Lambda}\Delta\boldsymbol{u} + \mathcal{A}_0(\boldsymbol{x})\Delta\boldsymbol{x} + \boldsymbol{R}_1(\boldsymbol{x},\boldsymbol{u},h) \tag{7}$$

Assumption 2: The control effectiveness matrix uncertainty satisfies $\|\tilde{\boldsymbol{\mathcal{B}}}_0(\boldsymbol{x})\hat{\boldsymbol{\mathcal{B}}}_0^{-1}(\boldsymbol{x})\| \le \bar{b} < 1$, where $\bar{b}$ is an unknown positive constant.

The inequality condition in Assumption 2 specifies a constraint on the uncertainties of the control effectiveness matrix. This (largest singular value) 2-norm constraint means the maximum magnification, which can be undergone by any vector when acted on by the control effectiveness uncertainties matrix $\tilde{\boldsymbol{\mathcal{B}}}_0(\boldsymbol{x})\hat{\boldsymbol{\mathcal{B}}}_0^{-1}(\boldsymbol{x})$, is smaller than 1. To be specific, this Note supposes that the uncertain control effort is less than the nominal control effort.

B. Fundamental Limitations of the INDI-SMC

The standard INDI-SMC law for stabilizing the error dynamics in Eq. (6) is designed as [21]

$$\begin{aligned}&\boldsymbol{u} = \boldsymbol{u}_0 + \Delta\boldsymbol{u}_{\text{indi-}s}, \quad \Delta\boldsymbol{u}_{\text{indi-}s} = \hat{\boldsymbol{\mathcal{B}}}_0^{-1}(\boldsymbol{x})\Big(\boldsymbol{v}_c + \boldsymbol{v}_s - \hat{\boldsymbol{y}}_0^{(\boldsymbol{\rho})}\Big),\\ &\boldsymbol{v}_c = -\boldsymbol{K}\boldsymbol{e} + \boldsymbol{y}_r^{(\boldsymbol{\rho})}, \quad \boldsymbol{v}_s = -\boldsymbol{K}_s\text{sgn}(\boldsymbol{\sigma})^\gamma\end{aligned} \tag{8}$$

where $\boldsymbol{K} \in \mathbb{R}^{m\times n}$ is designed such that $\boldsymbol{A}_c - \boldsymbol{B}_c\boldsymbol{K}$ is Hurwitz; $\gamma \in (0,1)$, $\boldsymbol{K}_s \in \mathbb{R}^{m\times m}$ is positive diagonal matrix; $\text{sgn}(\boldsymbol{\sigma})^\gamma = [|\sigma_1|^{\gamma_1}\text{sign}(\sigma_1),\ldots,|\sigma_m|^{\gamma_m}\text{sign}(\sigma_m)]^\top$; and $\hat{\boldsymbol{y}}_0^{(\boldsymbol{\rho})}$ is the measurement or estimation of $\boldsymbol{y}_0^{(\boldsymbol{\rho})}$. The sliding variable is designed as $\boldsymbol{\sigma} = \boldsymbol{S}\boldsymbol{e} - \boldsymbol{S}\boldsymbol{e}(0) + \int_0^t \boldsymbol{K}_o\boldsymbol{e}\,\text{d}\tau$, where $\boldsymbol{S} \in \mathbb{R}^{m\times n}$, $\boldsymbol{K}_o \in \mathbb{R}^{m\times n}$ with $\boldsymbol{K}_o = -\boldsymbol{S}(\boldsymbol{A}_c - \boldsymbol{B}_c\boldsymbol{K})$, and $\boldsymbol{S} = \text{diag}\{\boldsymbol{S}_i\}$, $\boldsymbol{S}_i = [K_{i,1},\ldots,K_{i,\rho_i-1},1] \in \mathbb{R}^{\rho_i}$. Substituting Eq. (8) into Eq. (6), we have

$$\dot{\boldsymbol{e}} = (\boldsymbol{A}_c - \boldsymbol{B}_c\boldsymbol{K})\boldsymbol{e} + \boldsymbol{B}_c\Big[\boldsymbol{v}_s + \Big(\boldsymbol{\mathcal{B}}_0(\boldsymbol{x})\hat{\boldsymbol{\mathcal{B}}}_0^{-1}(\boldsymbol{x}) - \boldsymbol{I}\Big)\Big(\boldsymbol{v}_c + \boldsymbol{v}_s - \hat{\boldsymbol{y}}_0^{(\rho)}\Big) + \tilde{\boldsymbol{y}}_0^{(\rho)} + \boldsymbol{\delta}(\boldsymbol{z}, h)\Big] \triangleq (\boldsymbol{A}_c - \boldsymbol{B}_c\boldsymbol{K})\boldsymbol{e} + \boldsymbol{B}_c(\boldsymbol{v}_s + \boldsymbol{\varepsilon}_{\text{indi-}s}) \tag{9}$$

in which $\tilde{\boldsymbol{y}}_0^{(\rho)} = \boldsymbol{y}_0^{(\rho)} - \hat{\boldsymbol{y}}_0^{(\rho)}$ and $\boldsymbol{\delta}(\boldsymbol{z}, h) = [\mathcal{A}_0(\boldsymbol{x})\Delta\boldsymbol{x} + \boldsymbol{R}_1(\boldsymbol{x}, \boldsymbol{u}, h)]|_{z=T(x_0), \boldsymbol{u}=\boldsymbol{u}_0+\Delta\boldsymbol{u}_{\text{indi-}s}}$.

Assumption 3: The measurement or estimation error of $\boldsymbol{y}_0^{(\rho)}$ is bounded, i.e., $\|\tilde{\boldsymbol{y}}_0^{(\rho)}\| \le \bar{\delta}_y$, where the constant $\bar{\delta}_y$ is the upper norm bound of $\tilde{\boldsymbol{y}}_0^{(\rho)}$.

Assumption 4 [21]: The term $\boldsymbol{\delta}(\boldsymbol{z}, h)$ in Eq. (9), which contains the closed-loop values of the expansion remainder $\boldsymbol{R}_1$ and $\mathcal{A}_0(\boldsymbol{x})\Delta\boldsymbol{x}$, is bounded, i.e., $\|\boldsymbol{\delta}(\boldsymbol{z}, h)\| \le \bar{\delta}_z$, where the constant $\bar{\delta}_z$ is the upper norm bound of $\boldsymbol{\delta}(\boldsymbol{z}, h)$.

These two assumptions are reasonable, which is explained as follows. The sensing error $\hat{\boldsymbol{y}}_0^{(\rho)}$, which is caused by noise, sensor dynamics, and sensor bias, is normally bounded [25]. Besides, if $\hat{\boldsymbol{y}}_0^{(\rho)}$ is estimated, the boundedness of estimation error is the basic requirement for the design of an estimator or filter [26,27]. Moreover, based on the analysis in [21,22], the value of $\|\boldsymbol{\delta}(\boldsymbol{z}, h)\|$ approaches zero as sampling frequency increases, and there always exists an h for guaranteeing the boundedness of $\|\boldsymbol{\delta}(\boldsymbol{z}, h)\|$.

From the closed-loop dynamics using INDI-SMC (Eq. (9)), it can be observed that the perturbation terms $\boldsymbol{\varepsilon}_{\text{indi-}s}$ influence the stability and performance. It is noteworthy that INDI-SMC in the literature does not consider sensing error, i.e., $\tilde{\boldsymbol{y}}_0^{(\rho)} = \boldsymbol{0}$ [21]. Furthermore, control reversal is also not considered by INDI-SMC, i.e., $\boldsymbol{\Lambda} \ne \boldsymbol{I}$. Denote $\boldsymbol{\Phi}_0(\boldsymbol{x}) = \boldsymbol{I} - \boldsymbol{\mathcal{B}}_0(\boldsymbol{x})\hat{\boldsymbol{\mathcal{B}}}_0^{-1}(\boldsymbol{x})$, and the following lemmas have been proved.

Lemma 1 [21]: If $\|\boldsymbol{\Phi}_0(\boldsymbol{x})\| \le \bar{b} < 1$, under Assumption 4, when $\tilde{\boldsymbol{y}}_0^{(\rho)} = \boldsymbol{0}$, for sufficiently high sampling frequency, the residual error $\boldsymbol{\varepsilon}_{\text{indi-}s}$ of INDI-SMC given by Eq. (9) is ultimately bounded as

$$\lim_{t\to\infty}\|\boldsymbol{\varepsilon}_{\text{indi-}s}\| \le \frac{\bar{\Delta}_{v_c}\bar{b} + \bar{\Delta}_{v_s}\bar{b} + \bar{\delta}_z}{1 - \bar{b}} \tag{10}$$

where $\bar{\Delta}_{v_c}$ and $\bar{\Delta}_{v_s}$ are the bounds of $\Delta\boldsymbol{v}_c = \boldsymbol{v}_c - \boldsymbol{v}_{c_0}$ and $\Delta\boldsymbol{v}_s = \boldsymbol{v}_s - \boldsymbol{v}_{s_0}$, respectively.

Lemma 2 [23]: If $\|\boldsymbol{\varepsilon}_{\text{indi-}s}\| \le \bar{\delta}_\varepsilon$ is satisfied for all $\boldsymbol{z} \in \mathbb{R}^n$, and $\dot{\boldsymbol{\eta}} = \boldsymbol{f}_{\text{in}}(\boldsymbol{\eta}, \boldsymbol{\xi})$ is input-to-state stable, then the state $\boldsymbol{z}$ in Eq. (3) is globally ultimately bounded by a class $\mathcal{K}$ function of $\bar{\delta}_\varepsilon$.

Remark 1: It can be observed from Lemmas 1 and 2 that $\|\boldsymbol{\Phi}_0(\boldsymbol{x})\| \le \bar{b} < 1$ is a critical sufficient condition for system stability. In practice, actuator faults and structural damage lead to changes in $\boldsymbol{\mathcal{B}}_0(\boldsymbol{x})$. In the absence of control reversal, i.e., $\boldsymbol{\Lambda} = \boldsymbol{I}$, then $\|\boldsymbol{\Phi}_0(\boldsymbol{x})\| \le \bar{b} < 1$ is equivalent to Assumption 2, which is naturally satisfied without requiring the adaptation of $\hat{\boldsymbol{\mathcal{B}}}_0(\boldsymbol{x})$ in many fault cases [21]. However, control reversal ($\boldsymbol{\Lambda} \ne \boldsymbol{I}$) violates $\|\boldsymbol{\Phi}_0(\boldsymbol{x})\| \le \bar{b} < 1$ even under Assumption 2. Consequently, both the boundedness of the residual error and the stability of the system cannot be guaranteed under of control of INDI-SMC. The INDI method also has promising disturbance rejection ability as discussed in [23]. The bounds of residual error and ultimate bounds of state are correlated to the bound of the disturbance variations [23].

Remark 2: The stability analysis of INDI-SMC also has limitations. First, sensing errors are not considered in INDI-SMC. Second, the variation bounds $\bar{\Delta}_{v_c}$, $\bar{\Delta}_{v_s}$, $\bar{\delta}_z$ are all influenced by the sampling frequency. However, the assumption of sufficiently high sampling frequency is used in Lemma 1 without presenting an explicit criterion for how high the sampling frequency should be.

III. Active Incremental Sliding Mode Control Against Control Reversal

An active incremental sliding mode control approach, denoted as A-INDI-SMC, will be proposed in this section. Its objective is to provide stable and desirable tracking even in the presence of control reversal. Moreover, an explicit and quantifiable expression for the ultimate bound of the tracking error, as a function of the sampling frequency and perturbation bounds, will be derived. The control structure of A-INDI-SMC is presented in Fig. 1. The FDI unit is used to identify the control direction by using a discrete-time incremental online FE approach.

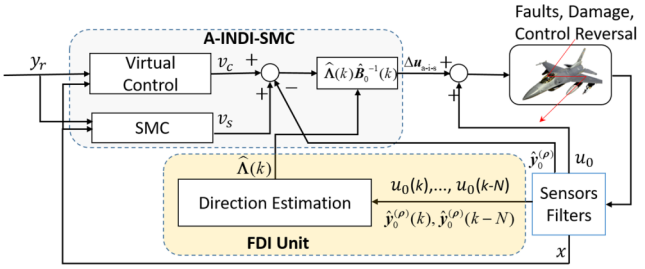

Fig. 1 The control structure of A-INDI-SMC.

Assumption 5: There is a minimum admissible time T_D between two consecutive sign switches of the diagonal elements of the matrix $\boldsymbol{\Lambda}$.

A. Fault Detection and Identification Design

In the presence of control reversal, reconstructing the changed sign promptly is essential. Therefore, the following FDI unit is introduced to identify the control direction matrix $\boldsymbol{\Lambda}$ online.

Using $\hat{\boldsymbol{\mathcal{B}}}_0(k)$, $\boldsymbol{\Phi}(k)$, $\tilde{\boldsymbol{y}}_0^{(\rho)}(k)$, $\hat{\boldsymbol{y}}^{(\rho)}(k)$, $\Delta\boldsymbol{u}(k)$, $\boldsymbol{R}_1(k)$, and $\mathcal{A}_0(k)$ to represent the value of $\hat{\boldsymbol{\mathcal{B}}}_0(\boldsymbol{x})$, $\boldsymbol{\Phi}_0(\boldsymbol{x})$, $\tilde{\boldsymbol{y}}_0^{(\rho)}$, $\hat{\boldsymbol{y}}^{(\rho)}$, $\Delta\boldsymbol{u}(t)$, $\boldsymbol{R}_1(\boldsymbol{x}, \boldsymbol{u}, h)$, and $\mathcal{A}_0(\boldsymbol{x})$ at $t = kh$, respectively, recall that $\boldsymbol{y}_0^{(\rho)}(k) = \hat{\boldsymbol{y}}_0^{(\rho)}(k) + \tilde{\boldsymbol{y}}_0^{(\rho)}(k)$, then Eq. (7) is written in a recursive way as

$$\hat{\boldsymbol{y}}_0^{(\rho)}(k+1) \triangleq \hat{\boldsymbol{y}}_0^{(\rho)}(k) + (\hat{\boldsymbol{\mathcal{B}}}_0(k) + \tilde{\boldsymbol{\mathcal{B}}}_0(k))\boldsymbol{\Lambda}(k)\Delta\boldsymbol{u}(k) + \mathcal{A}_0(k)\Delta\boldsymbol{x}(k) + \boldsymbol{R}_1(k) + \tilde{\boldsymbol{y}}_0^{(\rho)}(k) - \tilde{\boldsymbol{y}}_0^{(\rho)}(k+1) \tag{11}$$

In the above incremental dynamic equation, the first two terms on the right-hand side are more dominate than the rest. Therefore, define $\tilde{\boldsymbol{\delta}}_{\text{FDI}}(k) \triangleq \mathcal{A}_0(k)\Delta\boldsymbol{x}(k) + \boldsymbol{R}_1(k) + \tilde{\boldsymbol{y}}_0^{(\rho)}(k) - \tilde{\boldsymbol{y}}_0^{(\rho)}(k+1)$ as the lumped uncertainty term, then the dynamics in Eq. (11) can be rewritten as

$$\hat{\boldsymbol{y}}_0^{(\rho)}(k+1) = \hat{\boldsymbol{y}}_0^{(\rho)}(k) + (\hat{\boldsymbol{\mathcal{B}}}_0(k) + \tilde{\boldsymbol{\mathcal{B}}}_0(k))\boldsymbol{\Lambda}(k)\Delta\boldsymbol{u}(k) + \tilde{\boldsymbol{\delta}}_{\text{FDI}}(k) \tag{12}$$

From Eq. (12), it can be derived that

$$(\boldsymbol{I} + \hat{\boldsymbol{\mathcal{B}}}_0^{-1}(k)\tilde{\boldsymbol{\mathcal{B}}}_0(k))\boldsymbol{\Lambda}(k) = \hat{\boldsymbol{\mathcal{B}}}_0^{-1}(k)\Big(\hat{\boldsymbol{y}}_0^{(\rho)}(k+1) - \hat{\boldsymbol{y}}_0^{(\rho)}(k) - \tilde{\boldsymbol{\delta}}_{\text{FDI}}(k)\Big)(\Delta\boldsymbol{u}(k))^\dagger \tag{13}$$

where $(\Delta\boldsymbol{u}(k))^\dagger$ is the pseudoinverse of $\Delta\boldsymbol{u}(k)$. Under Assumption 2, the diagonal elements of $(\boldsymbol{I} + \hat{\boldsymbol{\mathcal{B}}}_0^{-1}(k)\tilde{\boldsymbol{\mathcal{B}}}_0(k))$ are positive. Using the diagonal matrix characteristics of $\boldsymbol{\Lambda}$, and considering $\tilde{\boldsymbol{\delta}}_{\text{FDI}}$ as an uncertainty, then the sign of $\boldsymbol{\Lambda}$ is derived from Eq. (13) as

$$\hat{w}_i(k) = \text{sign}\Big[\Big(\hat{\boldsymbol{\mathcal{B}}}_0^{-1}(k)\Big(\hat{\boldsymbol{y}}_0^{(\rho)}(k+1) - \hat{\boldsymbol{y}}_0^{(\rho)}(k)\Big)(\Delta\boldsymbol{u}(k))^\dagger\Big)_{i,i}\Big], \quad \forall i = 1, 2, \ldots, m \tag{14}$$

in which the subscript $(\cdot)_{i,i}$ denotes the ith diagonal element of a matrix; $\hat{w}_i(k)$ is the identified control direction of the ith actuator. Denote the ith row of the matrix $\hat{\boldsymbol{\mathcal{B}}}_0^{-1}(k)$ as $\boldsymbol{b}_i \in \mathbb{R}^{1\times m}$ and denote the ith element of the vector $(\Delta\boldsymbol{u}(k))^\dagger$ as $h_{u_i} \in \mathbb{R}$, then the estimation of w_i in Eq. (14) is simplified to $\hat{w}_i(k) = \text{sign}[\boldsymbol{b}_i(k)(\hat{\boldsymbol{y}}_0^{(\rho)}(k+1) - \hat{\boldsymbol{y}}_0^{(\rho)}(k))h_{u_i}(k)]$. Analogously, considering uncertainty, the real value of w_i is $\text{sign}[\boldsymbol{b}_i(k)(\hat{\boldsymbol{y}}_0^{(\rho)}(k+1) - \hat{\boldsymbol{y}}_0^{(\rho)}(k) - \tilde{\boldsymbol{\delta}}_{\text{FDI}}(k))h_{u_i}(k)]$. Therefore, the estimation in Eq. (14) leads to the following error:

$$\tilde{w}_i(k) = \Big(\text{sign}\Big[\boldsymbol{b}_i(k)\Big(\hat{\boldsymbol{y}}_0^{(\rho)}(k+1) - \hat{\boldsymbol{y}}_0^{(\rho)}(k) - \tilde{\boldsymbol{\delta}}_{\text{FDI}}(k)\Big)\Big] - \text{sign}\Big[\boldsymbol{b}_i(k)\Big(\hat{\boldsymbol{y}}_0^{(\rho)}(k+1) - \hat{\boldsymbol{y}}_0^{(\rho)}(k)\Big)\Big]\Big)\text{sign}[h_{u_i}(k)] \quad (15)$$

where $\tilde{w}_i = w_i - \hat{w}_i$. In case that $|\boldsymbol{b}_i(k)(\hat{\boldsymbol{y}}_0^{(\rho)}(k+1) - \hat{\boldsymbol{y}}_0^{(\rho)}(k))| > |\boldsymbol{b}_i(k)\tilde{\boldsymbol{\delta}}_{\text{FDI}}(k)|$, we have $\tilde{w}_i(k) = 0$. In other words, w_i is accurately identified by Eq. (14). Otherwise, incorrect identification of control direction could happen. Under Assumptions 3 and 4, $\|\tilde{\boldsymbol{\delta}}_{\text{FDI}}(k)\| < \bar{\delta}_z + \bar{\delta}_y$. Therefore, the condition $|\boldsymbol{b}_i(k)(\hat{\boldsymbol{y}}_0^{(\rho)}(k+1) - \hat{\boldsymbol{y}}_0^{(\rho)}(k))| > (\bar{\delta}_z + \bar{\delta}_y)\|\boldsymbol{b}_i(k)\|_1$ guarantees a correct sign identification using Eq. (14).

In the literature, it is widely assumed that $\tilde{\boldsymbol{y}}_0^{(\rho)} = \boldsymbol{0}$ [22,23,28]. This simplification leads to the FDI condition: $|\boldsymbol{b}_i(k)(\hat{\boldsymbol{y}}k_0^{(\rho)}(k+1) - \hat{\boldsymbol{y}}_0^{(\rho)}(k))| > \bar{\delta}_z\|\boldsymbol{b}_i(k)\|_1$. Since $\bar{\delta}_z$ approaches zero as h decreases [23], this condition can be easily satisfied under high sampling rate. However, if the measurement is corrupted by sensory noise and biases, it is possible that $\tilde{\boldsymbol{y}}_0^{(\rho)}$ becomes comparable to the term $\hat{\boldsymbol{y}}_0^{(\rho)}(k+1) - \hat{\boldsymbol{y}}_0^{(\rho)}(k)$, which would lead to incorrect identification in $\hat{w}_i(k)$. Assume that the control effectiveness $\boldsymbol{\mathcal{B}}_0(\boldsymbol{x})$ is slowly time varying, i.e., $\hat{\boldsymbol{\mathcal{B}}}_0(k) \approx \hat{\boldsymbol{\mathcal{B}}}_0(k-i)$, $\boldsymbol{\Lambda}(k) \approx \boldsymbol{\Lambda}(k-i)$, $i = 1, \ldots, N$, then we evaluate the dynamics in Eq. (12) at the previous N time step and surmise them together, which leads to

$$(\boldsymbol{I} + \hat{\boldsymbol{\mathcal{B}}}_0^{-1}(k)\tilde{\boldsymbol{\mathcal{B}}}_0(k))\boldsymbol{\Lambda}(k)\sum_{j=1}^{N}\Delta\boldsymbol{u}(k-j) \approx \hat{\boldsymbol{\mathcal{B}}}_0^{-1}(k)\Big(\hat{\boldsymbol{y}}_0^{(\rho)}(k) - \hat{\boldsymbol{y}}_0^{(\rho)}(k-N)\Big) - \hat{\boldsymbol{\mathcal{B}}}_0^{-1}(k)\sum_{j=1}^{N}\tilde{\boldsymbol{\delta}}_{\text{FDI}}(k-i) \quad (16)$$

Using Eq. (16), the sign identification law in Eq. (14) is updated to

$$\hat{w}_i(k) = \begin{cases} \text{sign}\Big[\Big(\hat{\boldsymbol{\mathcal{B}}}_0^{-1}(k)\Big(\hat{\boldsymbol{y}}_0^{(\rho)}(k) - \hat{\boldsymbol{y}}_0^{(\rho)}(k-N)\Big)\boldsymbol{H}_N(k)\Big)_{i,i}\Big], & t - t_e > \tau_d \\ \hat{w}_i(k-1), & \text{otherwise} \end{cases} \quad (17)$$

in which the dwell-time condition [29] is introduced to manage the transient behaviors. The step N is selected to satisfy $Nh < T_D$; $\boldsymbol{H}_N(k)$ is the pseudoinverse of $\sum_{j=1}^{N}\Delta\boldsymbol{u}(k-j)$; t_e is the previous instant when the control sign change is detected; $\tau_d > 0$ is the dwell-time constant. The complete identified matrix is therefore $\hat{\boldsymbol{\Lambda}} = \text{diag}\{\hat{w}_1, \hat{w}_2, \ldots, \hat{w}_m\}$. The selection of N and τ_d is related to system dynamics. For fast dynamics, their values should be relatively smaller. The condition for correctly identifying $\hat{\boldsymbol{\Lambda}}$ even in the presence of $\tilde{\boldsymbol{\delta}}_{\text{FDI}}$ is updated as

$$\Big|\boldsymbol{b}_i(k)\Big(\hat{\boldsymbol{y}}_0^{(\rho)}(k) - \hat{\boldsymbol{y}}_0^{(\rho)}(k-N)\Big)\Big| > (\bar{\delta}_z + \bar{\delta}_y)N\|\boldsymbol{b}_i(k)\|_1 \quad (18)$$

Remark 3: In most aircraft fault scenarios, Eq. (18) can be easily satisfied. Even if the sign identification of w_i cannot instantaneously follow the real one, the system will remain stable if the incorrect identify period is small as compared to the period without identification error [15,29]. It is worth noting that the control inputs will increase along with the wrong estimation of control sign. After that, the increment of $\boldsymbol{y}_0^{(\rho)}$ will also increase toward satisfying the condition in Eq. (18). Therefore, the condition for correctly identifying $\hat{\boldsymbol{\Lambda}}$ will be satisfied after a transient interval.

B. A-INDI-SMC Design

Based on the identified control direction $\hat{\boldsymbol{\Lambda}}$, this subsection presents the A-INDI-SMC law. Using Eq. (7), the error dynamics in Eq. (6) becomes

$$\dot{\boldsymbol{e}} = \boldsymbol{A}_c\boldsymbol{e} + \boldsymbol{B}_c\Big(\boldsymbol{y}_0^{(\rho)} + (\hat{\boldsymbol{\mathcal{B}}}_0(\boldsymbol{x}) + \tilde{\boldsymbol{\mathcal{B}}}_0(\boldsymbol{x}))\boldsymbol{\Lambda}\Delta\boldsymbol{u} + \mathcal{A}_0(\boldsymbol{x})\Delta\boldsymbol{x} + \boldsymbol{R}_1(\boldsymbol{x},\boldsymbol{u},h) - \boldsymbol{y}_r^{(\rho)}\Big) \quad (19)$$

which can be discretized using Euler's forward approximation as

$$\boldsymbol{e}(k+1) = [\boldsymbol{I} + h\boldsymbol{A}_c]\boldsymbol{e}(k) + h\boldsymbol{B}_c\Big(\boldsymbol{y}_0^{(\rho)}(k) + (\hat{\boldsymbol{\mathcal{B}}}_0(k) + \tilde{\boldsymbol{\mathcal{B}}}_0(k))\boldsymbol{\Lambda}(k)\Delta\boldsymbol{u}(k) + \mathcal{A}_0(k)\Delta\boldsymbol{x}(k) + \boldsymbol{R}_1(k) - \boldsymbol{y}_r^{(\rho)}(k)\Big) \quad (20)$$

The discrete-time active incremental sliding mode control is proposed as

$$\Delta\boldsymbol{u}_{a-i-s}(k) = \hat{\boldsymbol{\Lambda}}(k)\hat{\boldsymbol{\mathcal{B}}}_0^{-1}(k)\Big(\boldsymbol{v}_c(k) + \boldsymbol{v}_s(k) - \hat{\boldsymbol{y}}_0^{(\rho)}(k)\Big) \quad (21)$$

where the identification of $\hat{\boldsymbol{\Lambda}}(k)$ has been discussed in Sec. III.A. The nominal virtual control is designed as $\boldsymbol{v}_c(k) = -\boldsymbol{K}\boldsymbol{e}(k) + \boldsymbol{y}_r^{(\rho)}(k)$ for stabilizing the unperturbed system and $\boldsymbol{v}_s$ is designed for perturbation compensations. Design the discrete sliding variable $\boldsymbol{\sigma}(\boldsymbol{e}): \mathbb{R}^n \to \mathbb{R}^m$ as

$$\boldsymbol{\sigma}(k) = \boldsymbol{S}\boldsymbol{e}(k) - \boldsymbol{S}\boldsymbol{e}(0) + \boldsymbol{E}_I(k), \quad \boldsymbol{E}_I(k) = \boldsymbol{E}_I(k-1) + \boldsymbol{K}_e\boldsymbol{e}(k-1) \quad (22)$$

where $\boldsymbol{K}_e = -h\boldsymbol{S}(\boldsymbol{A}_c - \boldsymbol{B}_c\boldsymbol{K})$. Consider the motions on the sliding surface, i.e., $\boldsymbol{\sigma}(k+1) = \boldsymbol{\sigma}(k) = 0$; then using Eqs. (20) and (22), the following equations are derived:

$$\begin{cases} \boldsymbol{S}(\boldsymbol{I} + h\boldsymbol{A}_c)\boldsymbol{e}(k) - \boldsymbol{S}\boldsymbol{e}(0) + \boldsymbol{E}_I(k+1) + h\boldsymbol{S}\boldsymbol{B}_c\Big(\boldsymbol{y}_0^{(\rho)}(k) + \boldsymbol{\mathcal{B}}_0(k)\Delta\boldsymbol{u}(k) + \mathcal{A}_0(k)\Delta\boldsymbol{x}(k) + \boldsymbol{R}_1(k) - \boldsymbol{y}_r^{(\rho)}(k)\Big) = 0 \\ \boldsymbol{S}\boldsymbol{e}(k) - \boldsymbol{S}\boldsymbol{e}(0) + \boldsymbol{E}_I(k) = 0, \quad \boldsymbol{E}_I(k+1) = \boldsymbol{E}_I(k) + \boldsymbol{K}_e\boldsymbol{e}(k) \end{cases} \quad (23)$$

Using Eq. (23), the equivalent control [7] is calculated by

$$\Delta\boldsymbol{u}_{\text{eq}}(k) = \boldsymbol{\mathcal{B}}_0^{-1}(k)\Big(\boldsymbol{y}_r^{(\rho)}(k) - \boldsymbol{K}\boldsymbol{e}(k) - \boldsymbol{y}_0^{E}(k) - \boldsymbol{\delta}(k)\Big) \quad (24)$$

in which $\boldsymbol{\delta}(k) = [\mathcal{A}_0(\boldsymbol{x})\Delta\boldsymbol{x} + \boldsymbol{R}_1(\boldsymbol{x},\boldsymbol{u},h)]|_{\boldsymbol{u}=\boldsymbol{u}_0(k)+\Delta\boldsymbol{u}_{a-i-s}(k)}$. Substitute Eq. (24) into Eq. (20), the ideal sliding mode dynamic equation results in $\boldsymbol{e}(k+1) = [\boldsymbol{I} + h(\boldsymbol{A}_c - \boldsymbol{B}_c\boldsymbol{K})]\boldsymbol{e}(k)$, which indicates that, on the sliding surface, the desired error dynamics are achieved, which ensures that $\boldsymbol{e}$ converges to zero and $\boldsymbol{\xi} \to \boldsymbol{r}$. To compensate for uncertainties and disturbances, the sliding mode virtual control $\boldsymbol{v}_s$ is designed as $\boldsymbol{v}_s(k) = -\boldsymbol{K}_s\text{sgn}(\boldsymbol{\sigma}(k))^{\gamma} = -[K_{s,1}|\sigma_1(k)|^{\gamma}\text{sign}(\sigma_1(k)), \ldots, K_{s,m}|\sigma_m(k)|^{\gamma}\text{sign}(\sigma_m(k))]^{\top}$, where $K_{s,i} > 0, \gamma \in (0,1), i = 1, \ldots, m$.

C. Stability and Robustness Analysis

The stability and robustness of the A-INDI-SMC method in the presence of control reversal, model uncertainties, and sensing errors will be analyzed in this subsection.

Theorem 1: Under Assumptions 2–5, if $\boldsymbol{f}_{\text{in}}(\boldsymbol{\eta},\boldsymbol{\xi})$ is continuously differentiable and globally Lipschitz in $(\boldsymbol{\eta},\boldsymbol{\xi})$, and the origin of $\dot{\boldsymbol{\eta}} = \boldsymbol{f}_{\text{in}}(\boldsymbol{\eta},\boldsymbol{0})$ is globally exponentially stable, then using the proposed control law in Eq. (21), the tracking error $\boldsymbol{e}$ in Eq. (19) converges to an arbitrary small bound, while the internal state $\boldsymbol{\eta}$ in Eq. (3) is globally ultimately bounded.

Proof 1: Assume that the system satisfies the identifiable condition in Eq. (18), then $\boldsymbol{\Lambda}(k)\hat{\boldsymbol{\Lambda}}(k) = \boldsymbol{I}$ holds on. Substituting Eq. (21) and Eq. (20) into Eq. (22) yields

$$\begin{aligned}\boldsymbol{\sigma}(k+1) &= \boldsymbol{S}[\boldsymbol{I}+h\boldsymbol{A}_c]\boldsymbol{e}(k) - \boldsymbol{S}\boldsymbol{e}(0) + \boldsymbol{E}_I(k) + \boldsymbol{K}_e\boldsymbol{e}(k)\\ &\quad + h\boldsymbol{S}\boldsymbol{B}_c\Big(\boldsymbol{y}_0^{(\rho)}(k) + (\hat{\boldsymbol{\mathcal{B}}}_0(k)+\tilde{\boldsymbol{\mathcal{B}}}_0(k))\boldsymbol{\Lambda}(k)\hat{\boldsymbol{\Lambda}}(k)\hat{\boldsymbol{\mathcal{B}}}_0^{-1}(k)\\ &\quad \times\Big(\boldsymbol{v}_c(k)+\boldsymbol{v}_s(k)-\hat{\boldsymbol{y}}_0^{(\rho)}(k)\Big)+\boldsymbol{\delta}(k)-\boldsymbol{y}_r^{(\rho)}(k)\Big)\\ &= \boldsymbol{\sigma}(k) + h\boldsymbol{S}\boldsymbol{B}_c\Big(-\boldsymbol{K}_s\mathrm{sgn}(\boldsymbol{\sigma}(k))^{\gamma}+\tilde{\boldsymbol{\mathcal{B}}}_0(k)\hat{\boldsymbol{\mathcal{B}}}_0^{-1}(k)\\ &\quad \times\Big(\boldsymbol{v}_c(k)+\boldsymbol{v}_s(k)-\hat{\boldsymbol{y}}_0^{(\rho)}\Big)+\tilde{\boldsymbol{y}}_0^{(\rho)}(k)+\boldsymbol{\delta}(k)\Big) \qquad (25)\end{aligned}$$

Denote $\tilde{\boldsymbol{\mathcal{B}}}_0(k)\hat{\boldsymbol{\mathcal{B}}}_0^{-1}(k) \triangleq \boldsymbol{\Phi}_s(k)$ and $\tilde{\boldsymbol{y}}_0^{(\rho)}(k)+\boldsymbol{\delta}(k) \triangleq \tilde{\Delta}_s(k)$, then using the controller in Eq. (21) leads to

$$\begin{aligned}\boldsymbol{y}^{(\rho)}(k) &= \boldsymbol{v}_c(k)+\boldsymbol{v}_s(k)+\tilde{\boldsymbol{\Delta}}_s(k)+\boldsymbol{\Phi}_s(k)\Big(\boldsymbol{v}_c(k)+\boldsymbol{v}_s(k)-\hat{\boldsymbol{y}}_0^{(\rho)}(k)\Big)\\ &\triangleq \boldsymbol{v}_c(k)+\boldsymbol{v}_s(k)+\boldsymbol{\varepsilon}_{a-i-s}(k) \qquad (26)\end{aligned}$$

Analogous to the derivations in [21], and using Eq. (26), the residual cancellation error of A-INDI-SMC follows:

$$\begin{aligned}\boldsymbol{\varepsilon}_{a-i-s}(k) &= \boldsymbol{\Phi}_s(k)\Big(\boldsymbol{v}_c(k)+\boldsymbol{v}_s(k)-\boldsymbol{v}_c(k-1)-\boldsymbol{v}_s(k-1)\\ &\quad -\boldsymbol{\varepsilon}_{a-i-s}(k-1)+\tilde{\boldsymbol{y}}_0^{(\rho)}(k)\Big)+\tilde{\boldsymbol{\Delta}}_s(k)\\ &= -\boldsymbol{\Phi}_s(k)\boldsymbol{\varepsilon}_{a-i-s}(k-1)+\boldsymbol{\Phi}_s(k)(\Delta\boldsymbol{v}_c(k)+\Delta\boldsymbol{v}_s(k))\\ &\quad +(\boldsymbol{I}+\boldsymbol{\Phi}_s(k))\tilde{\boldsymbol{y}}_0^{(\rho)}(k)+\boldsymbol{\delta}(k) \qquad (27)\end{aligned}$$

Referring to [30], the incremental terms $\Delta\boldsymbol{v}_c(k)$, $\Delta\boldsymbol{v}_s(k)$ are in the order of magnitude of $O(h^2)$. Under Assumption 2, $\|\boldsymbol{\Phi}_s(k)\| = \|\tilde{\boldsymbol{\mathcal{B}}}_0(k)\hat{\boldsymbol{\mathcal{B}}}_0^{-1}(k)\| \le \bar{b} < 1$. Recall that under Assumptions 3 and 4, $\|\tilde{\boldsymbol{y}}_0^{(\rho)}\| \le \bar{\delta}_y$ and $\|\boldsymbol{\delta}(z,h)\| \le \bar{\delta}_z$, and thus the residual error in Eq. (27) is derived as

$$\begin{aligned}\|\boldsymbol{\varepsilon}_{a-i-s}(k)\| &\le \bar{b}\|\boldsymbol{\varepsilon}_{a-i-s}(k-1)\| + \bar{b}\Big(\|\Delta\boldsymbol{v}_c(k)+\Delta\boldsymbol{v}_s(k)\|\Big)+\bar{\delta}_z\\ &\quad +(1+\bar{b})\bar{\delta}_y\\ &\le \bar{b}^k\|\boldsymbol{\varepsilon}_{a-i-s}(0)\| + \sum_{j=1}^{k}\Big[\bar{b}^j\|\Delta\boldsymbol{v}_c(j)+\Delta\boldsymbol{v}_s(j)\|\\ &\quad +\bar{b}^{(j-1)}\Big(\bar{\delta}_z+(1+\bar{b})\bar{\delta}_y\Big)\Big] \qquad (28)\end{aligned}$$

Using the sum formula of geometric series, it follows that

$$\begin{aligned}\|\boldsymbol{\varepsilon}_{a-i-s}(k+1)\| &\le \bar{b}^{k+1}\|\boldsymbol{\varepsilon}_{a-i-s}(0)\| + \Big(\bar{\Delta}_{v_c}+\bar{\Delta}_{v_s}\Big)\frac{\bar{b}-\bar{b}^{k+1}}{1-\bar{b}}\\ &\quad +\bar{\delta}_z\frac{1-\bar{b}^k}{1-\bar{b}}+\bar{\delta}_y\frac{(1-\bar{b}^k)(1+\bar{b})}{1-\bar{b}} \qquad (29)\end{aligned}$$

Using the fact that $\bar{b}<1$, we have $\lim_{k\to\infty}\|\boldsymbol{\varepsilon}_{a-i-s}\| \le [(\bar{\Delta}_{v_c}+\bar{\Delta}_{v_s})\bar{b}/1-\bar{b}] + (\bar{\delta}_z/1-\bar{b}) + [(1+\bar{b})\bar{\delta}_y/1-\bar{b}]$, which shows an explicit ultimately bound expression of $\boldsymbol{\varepsilon}_{a-i-s}$ as a function of the perturbation bounds $\bar{\delta}_z$, $\bar{\Delta}_{v_c}$, $\bar{\Delta}_{v_s}$, and the sensing error bound $\bar{\delta}_y$.

Following Eq. (25), the difference equation of $\boldsymbol{\sigma}(k)$ is

$$\Delta\boldsymbol{\sigma}(k) = \boldsymbol{\sigma}(k+1)-\boldsymbol{\sigma}(k) = h\boldsymbol{S}\boldsymbol{B}_c(-\boldsymbol{K}_s\mathrm{sgn}(\boldsymbol{\sigma}(k))^{\gamma}+\boldsymbol{\varepsilon}_{a-i-s}(k)) \qquad (30)$$

Then, each element of $\Delta\boldsymbol{\sigma}(k)$ is calculated as $\Delta\sigma_i(k) = h\varepsilon_{a-i-s,i}(k) - hK_{s,i}|\sigma_i(k)|^{\gamma}\mathrm{sign}(\sigma_i(k))$, where $\varepsilon_{a-i-s,i}$ is the ith element of $\boldsymbol{\varepsilon}_{a-i-s}$.

1) When the sliding variable $\sigma_i(k)>0$, this yields $\Delta\sigma_i(k) = -hK_{s,i}|\sigma_i(k)|^{\gamma} + h\varepsilon_{a-i-s,i}(k)$. It is observed that $\forall\sigma_i(k) \ge (|\varepsilon_{a-i-s,i}|/K_{s,i})^{1/\gamma}$, $\Delta\sigma_i(k)<0$, $\sigma_i(k)$ decreases, until it enters the range $0<\sigma_i(k)\le(|\varepsilon_{a-i-s,i}|/K_{s,i})^{1/\gamma}$.

2) When the sliding variable $\sigma_i(k)<0$, Eq. (30) becomes $\Delta\sigma_i(k) = hK_{s,i}|\sigma_i(k)|^{\gamma} + h\varepsilon_{a-i-s,i}(k)$. It is observed that $\forall\sigma_i(k) \le -(|\varepsilon_{a-i-s,i}|/K_{s,i})^{1/\gamma}$, $\Delta\sigma_i(k)>0$, $\sigma_i(k)$ increases, until it enters the range $-(|\varepsilon_{a-i-s,i}|/K_{s,i})^{1/\gamma} \le \sigma_i(k) < 0$.

Therefore, the controller leads to a quasi-sliding motion in a finite time T_1 with $|\sigma_i(k)| \le \bar{\delta}_{s,i} = (|\varepsilon_{a-i-s,i}|/K_{s,i})^{1/\gamma}$, whose size can be made arbitrarily small. Denote the sliding variable in a quasi-sliding motion as $\boldsymbol{\sigma}_{\mathrm{sm}} = [\sigma_{\mathrm{sm},1},\sigma_{\mathrm{sm},2},\ldots,\sigma_{\mathrm{sm},m}]^{\mathrm{T}}$, where $\boldsymbol{\sigma}_{\mathrm{sm},i}(k)$ has a magnitude of $O(\bar{\delta}_{s,i})$ due to the nonideal sliding motion. The quasi-sliding mode dynamics are

$$\begin{aligned}\boldsymbol{e}(k+1) &= [\boldsymbol{I}+h(\boldsymbol{A}_c-\boldsymbol{B}_c\boldsymbol{K})]\boldsymbol{e}(k)+h\boldsymbol{B}_c(\boldsymbol{v}_s(k)+\boldsymbol{\varepsilon}_{a-i-s}(k))\\ &= [\boldsymbol{I}+h(\boldsymbol{A}_c-\boldsymbol{B}_c\boldsymbol{K})]\boldsymbol{e}(k)+\boldsymbol{B}_c(\boldsymbol{S}\boldsymbol{B}_c)^{-1}\Delta\boldsymbol{\sigma}_{\mathrm{sm}}(k) \qquad (31)\end{aligned}$$

in which $\Delta\boldsymbol{\sigma}_{\mathrm{sm}}(k) = \boldsymbol{\sigma}_{\mathrm{sm}}(k+1)-\boldsymbol{\sigma}_{\mathrm{sm}}(k)$. Recall that $\rho(\boldsymbol{I}+h(\boldsymbol{A}_c-\boldsymbol{B}_c\boldsymbol{K})) = \bar{\lambda}<1$, where $\rho(\cdot)$ denotes the spectral radius of a matrix $(\cdot)\in\mathbb{R}^{n\times n}$. Then the inequation $\|\boldsymbol{e}(k+1)\| \le \bar{\lambda}\|\boldsymbol{e}(k)\| + \|\Delta\boldsymbol{\sigma}_{\mathrm{sm}}(k)\|$ holds because $\|\boldsymbol{B}_c(\boldsymbol{S}\boldsymbol{B}_c)^{-1}\| = 1$. During the sliding motion, we have $\|\Delta\boldsymbol{\sigma}_{\mathrm{sm}}(k)\| \le 2\sqrt{m}\bar{\delta}_s(k)$, where $\bar{\delta}_s(k) = \sup_{i=1,\ldots,m}(|\varepsilon_{a-i-s,i}(k)|/K_{s,i})^{1/\gamma}$. Define $\underline{K} = \inf_{i=1,\ldots,m}K_{s,i}$, then

$$\begin{aligned}\|\boldsymbol{e}(k_s+k+1)\| &\le \bar{\lambda}\|\boldsymbol{e}(k_s+k)\| + 2\sqrt{m}\bar{\delta}_s(k)\\ &\le \bar{\lambda}^{k_s+1}\|\boldsymbol{e}(k)\| + \frac{1-\bar{\lambda}^{k_s}}{1-\bar{\lambda}}2\sqrt{m}\left(\frac{\|\boldsymbol{\varepsilon}_{a-i-s}(k)\|}{\underline{K}}\right)^{1/\gamma} \qquad (32)\end{aligned}$$

Substituting Eq. (29) into Eq. (32), and using the fact that $\lim_{k\to\infty}\bar{b}^k\to 0$ and $\lim_{k_s\to\infty}\bar{\lambda}^k\to 0$ lead to

$$\lim_{k\to\infty}\|\boldsymbol{e}(k)\| \le \frac{2\sqrt{m}}{1-\bar{\lambda}}\left(\frac{(\bar{\Delta}_{v_c}+\bar{\Delta}_{v_s})\bar{b}+\bar{\delta}_z+(1+\bar{b})\bar{\delta}_y}{\underline{K}(1-\bar{b})}\right)^{1/\gamma} \triangleq \varepsilon^{\star} \qquad (33)$$

Equation (33) provides an explicit expression of the ultimate bound of the tracking error $\boldsymbol{e}$ as a function of $\bar{b}$, the sampling interval h, the spectral radius of $\boldsymbol{A}_c-\boldsymbol{B}_c\boldsymbol{K}$, the sensing error bound $\bar{\delta}_y$, and the sampling interval-related perturbation bounds $\bar{\delta}_z$, $\bar{\Delta}_{v_c}$, and $\bar{\Delta}_{v_s}$. Since the reference signal $\boldsymbol{r}$ is designed to be bounded, i.e., $\|\boldsymbol{r}\|<\bar{r}$, Eq. (33) also leads to a bounded external state $\boldsymbol{\xi}$.

Regarding the internal dynamics, choose $V_{\mathrm{in}}(\boldsymbol{\eta})$ defined in $D_\eta = \{\boldsymbol{\eta}\in\mathbb{R}^{n-n_e}\}$ as the candidate Lyapunov function for $\dot{\boldsymbol{\eta}} = \boldsymbol{f}_{\mathrm{in}}(\boldsymbol{\eta},\boldsymbol{\xi})$. Since the origin $\dot{\boldsymbol{\eta}} = \boldsymbol{f}_{\mathrm{in}}(\boldsymbol{\eta},\boldsymbol{0})$ is globally exponentially stable, then there exists class $\mathcal{K}_\infty$ functions α_1' and α_2' such that $\alpha_1'(\|\boldsymbol{\eta}\|) \le \|V_{\mathrm{in}}(\boldsymbol{\eta})\| \le \alpha_2'(\|\boldsymbol{\eta}\|)$ is satisfied. In the meanwhile, $V_{\mathrm{in}}(\boldsymbol{\eta})$ satisfies $(\partial V_{\mathrm{in}}/\partial\boldsymbol{\eta})\boldsymbol{f}_{\mathrm{in}}(\boldsymbol{\eta},\boldsymbol{0}) \le -c_3\|\boldsymbol{\eta}\|^2$, $\|\partial V_{\mathrm{in}}/\partial\boldsymbol{\eta}\| \le c_4\|\boldsymbol{\eta}\|$ for some positive constants c_3 and c_4. Because $\boldsymbol{f}_{\mathrm{in}}(\boldsymbol{\eta},\boldsymbol{\xi})$ is continuously differentiable and globally Lipschitz in $(\boldsymbol{\eta},\boldsymbol{\xi})$, then there exists a global Lipschitz constant L such that $\|\boldsymbol{f}_{\mathrm{in}}(\boldsymbol{\eta},\boldsymbol{\xi})-\boldsymbol{f}_{\mathrm{in}}(\boldsymbol{\eta},\boldsymbol{0})\| \le L(\|\boldsymbol{e}\|+\|\boldsymbol{r}\|)$, $\forall\,\boldsymbol{\eta}\in\mathbb{R}^{n-n_e}$. As a result, the time derivative of $V_{\mathrm{in}}(\boldsymbol{\eta})$ satisfies [23]

$$\begin{aligned}\dot{V}_{\mathrm{in}}(\boldsymbol{\eta}) &= \frac{\partial V_{\mathrm{in}}}{\partial\boldsymbol{\eta}}\boldsymbol{f}_{\mathrm{in}}(\boldsymbol{\eta},\boldsymbol{\xi})\\ &\le \frac{\partial V_{\mathrm{in}}}{\partial\boldsymbol{\eta}}\boldsymbol{f}_{\mathrm{in}}(\boldsymbol{\eta},\boldsymbol{0})+\left\|\frac{\partial V_{\mathrm{in}}}{\partial\boldsymbol{\eta}}\right\|\|\boldsymbol{f}_{\mathrm{in}}(\boldsymbol{\eta},\boldsymbol{\xi})-\boldsymbol{f}_{\mathrm{in}}(\boldsymbol{\eta},\boldsymbol{0})\|\\ &\le -c_3\|\boldsymbol{\eta}\|^2 + c_4L\|\boldsymbol{\eta}\|(\|\boldsymbol{e}\|+\|\boldsymbol{r}\|)\\ &\le -c_3(1-\theta_1)\|\boldsymbol{\eta}\|^2, \quad \forall\,\|\boldsymbol{\eta}\| \ge \frac{c_4L(\|\boldsymbol{e}\|+\|\boldsymbol{r}\|)}{c_3\theta_1} \qquad (34)\end{aligned}$$

with constant $\theta_1\in(0,1)$. Denote the initial time point as t_0, and $\mu \triangleq (c_4L/c_3\theta_1)(\sup_{t_0+T_1\le\tau\le t}(\|\boldsymbol{e}\|+\|\boldsymbol{r}\|))$. As a result, there exists a class $\mathcal{KL}$ function β' such that $\|\boldsymbol{\eta}\| \le \beta'(\|\boldsymbol{\eta}(t_0+T_1)\|, t-t_0-T_1) + \alpha_1'^{-1}(\alpha_2'(\mu))$, $\forall t\ge t_0+T_1$. Analogous to the results in [23], the normal value of the internal state satisfies

$$\|\boldsymbol{\eta}\| \le \theta_2\varepsilon^\star + \alpha_1'^{-1}\left(\alpha_2'\left(\frac{c_4 L}{c_3\theta_1}(\varepsilon^\star + \bar{r})\right)\right), \quad \forall t \ge t_0 + T_1 + T_2 \tag{35}$$

for some finite $T_2 > 0$ and $\theta_2 > 0$. This shows that $\boldsymbol{\eta}$ is globally ultimately bounded by a class $\mathcal{K}$ function of $\varepsilon^\star$ and $\bar{r}$. This completes the proof. □

Remark 4: For the nonlinear system modeled in Eq. (7), the term $\boldsymbol{\Phi}_0(\boldsymbol{x})$ equals $\boldsymbol{I} - (\hat{\boldsymbol{\mathcal{B}}}_0(x) + \tilde{\boldsymbol{\mathcal{B}}}_0(x))\boldsymbol{\Lambda}\hat{\boldsymbol{\mathcal{B}}}_0^{-1}(x)$. It can be observed that if $\exists i$, $w_i = -1$, then $\rho(\boldsymbol{\Phi}_0(\boldsymbol{x})) > 1$. As a consequence, the boundedness of the perturbation term in Eq. (9), as well as the closed-loop stability of INDI-SMC presented in Sec. II.B, cannot be guaranteed. By contrast, the newly proposed A-INDI-SMC has boarder applicability. This is because even if $\exists i$, $w_i = -1$, with the help of FDI in Sec. III.A, $\boldsymbol{\Lambda}(k)\hat{\boldsymbol{\Lambda}}(k) = \boldsymbol{I}$ in Eq. (25). Consequently, $\boldsymbol{\varepsilon}_{a-i-s}(k)$ in Eq. (27) is bounded under Assumption 2, which further leads to guaranteed closed-loop stability.

Remark 5: In the case of $\boldsymbol{\Lambda}(k)\hat{\boldsymbol{\Lambda}}(k) \ne \boldsymbol{I}$, the system will remain stable under very short incorrect identification intervals, which is explained as follows. In the activating period of unstable mode, the sliding variable $\Delta\sigma_i(k) = hK_{s,i}|\sigma_i(k)|^\gamma \mathrm{sign}(\sigma_i(k)) + h\varepsilon_{a-i-s,i}(k)$. Suppose that the unmatched sign identification happens in the transient internal $[k_f, k_R)$. Denote the upper bound of $|\varepsilon_{a-i-s,i}(k)|$ in this period as $\bar{\varepsilon}$. Denote $\mathbb{M}_s$ as the set of stable modes, and $\mathbb{M}_u$ represents the set of unstable mode. Suppose that $\lambda_1 = \min(hK_{s,i}|\sigma_i(k)|^\gamma - h\bar{\varepsilon})$, $k \in \mathbb{M}_s$ is the minimal rate of decay in the stable mode, and $\lambda_2 = \max(hK_{s,i}|\sigma_i(k)|^\gamma + h\bar{\varepsilon})$, $k \in \mathbb{M}_u$ is the maximum rate of growth in the unstable mode. Then, for any $k \in [k_f, k_R)$, from the differential inequality theory, one has $|\sigma_i(k + k_f)| \le |\sigma_i(k_f)| - \lambda_1 T_s + \lambda_2 T_u$, where T_s and T_u represent the activating period for stable modes, and the activating period of unstable mode, respectively. Consequently, if the incorrectly identified intervals satisfy $T_u < (\lambda_1/\lambda_2)T_s$, then $|\sigma_i(k + k_f)| \le |\sigma_i(k_f)|$. In conclusion, the system will remain stable if the activating period of the correctly identified w_i is long enough compared with that of the unmatched intervals [15]. That is to say the energy stored during a transient interval with a wrong identification can be extracted in the longer stable intervals for continuous systems under bounded inputs [29].

Remark 6: In the literature, the term $\boldsymbol{y}_0^{(\boldsymbol{\rho})}$ is often assumed to be accurately known [22,23,28]. Although in observer-based control methods the estimation error term $\tilde{\boldsymbol{y}}_0^{(\boldsymbol{\rho})}$ is often dropped out for the convenience of control design [23,31], it should be kept in the closed-loop system equations for rigorous stability and robustness analysis. By contrast, the impacts of $\tilde{\boldsymbol{y}}_0^{(\boldsymbol{\rho})}$ on the closed-loop dynamics have been explicitly considered in the preceding analysis.

Remark 7: The explicit and quantifiable expression in Eq. (33) also makes it possible to select a sampling interval h based on the tracking performance requirement, instead of weakly assuming the sampling frequency to be sufficiently high [21]. In general, the incremental perturbation bounds $\bar{\delta}_z$, $\bar{\Delta}_{v_c}$ are inversely correlated to h; thus reducing h is beneficial for performance enhancement if hardware permits. Given a prescribed tracking performance requirement, i.e., $\lim_{k\to\infty}\|\boldsymbol{e}(k+1)\|$, and with the pre-estimation of the upper bounds of the uncertainties, then the control parameters and the sampling interval h can be selected using Eq. (33).

IV. Numerical Validations

In this section, the proposed A-INDI-SMC method will be validated by an aircraft FTC problem, considering sensing errors, control reversal, model uncertainties, actuator faults, and structural damage.

A. Fault-Tolerant Flight Control Design

The actuator fault cases considered in this Note include loss of control surface area, control surface jamming, and the oscillatory failure cases (OFCs). Referring to the investigations in [21,24], structural damage may lead to changes in aerodynamic properties, inertia properties, and control effectiveness. An attitude control system is designed to make an aircraft robustly track the references of roll angle ϕ and pitch angle θ while minimizing the sideslip angle β. Denote the roll, pitch, and yaw rates as $\boldsymbol{\omega} = [p, q, r]^\top$. The control inputs have aileron deflection δ_a, elevator deflection δ_e, and rudder deflection δ_r. Consequently, the controlled variables are chosen as $\boldsymbol{y} = [\phi, \theta, \beta]^\top$. The nonlinear attitude dynamics of an aircraft with $\boldsymbol{x}_1 = [\phi, \theta, \beta]^\top, \boldsymbol{x}_2 = [p, q, r]^\top, \boldsymbol{x} = [\boldsymbol{x}_1^\top, \boldsymbol{x}_2^\top]^\top$, and control input $\boldsymbol{u} = [\delta_a, \delta_e, \delta_r]^\top$ are given as [21,23]

$$\begin{cases} \dot{\boldsymbol{x}}_1 = \boldsymbol{f}_1(\boldsymbol{x}) + \boldsymbol{g}_1(\boldsymbol{x}_1)\boldsymbol{x}_2 \\ \dot{\boldsymbol{x}}_2 = (1-\kappa)\boldsymbol{f}_2(\boldsymbol{x}) + \kappa\boldsymbol{f}_2'(\boldsymbol{x}) + (1-\kappa)\boldsymbol{g}_2(\boldsymbol{x})\boldsymbol{u} + \kappa\boldsymbol{g}_2'(\boldsymbol{x})\boldsymbol{u} \end{cases} \tag{36}$$

where $\kappa \in [0, 1]$ is designed as a unit step function to indicate sudden faults that happened during the flight. The prefault dynamics $\boldsymbol{f}_1(\boldsymbol{x}_1)$, $\boldsymbol{g}_1(\boldsymbol{x}_1)$ can be found in [22], while the postfault dynamics are

$$\boldsymbol{f}_2'(\boldsymbol{x}) = \left(\frac{1}{m'}\tilde{\boldsymbol{S}}\tilde{\boldsymbol{S}} + \boldsymbol{J}'\right)^{-1}\left(\tilde{\boldsymbol{S}}\tilde{\boldsymbol{\omega}}\boldsymbol{V} - \frac{1}{m'}\tilde{\boldsymbol{S}}\tilde{\boldsymbol{\omega}}\tilde{\boldsymbol{S}}\boldsymbol{\omega} - \tilde{\boldsymbol{V}}\tilde{\boldsymbol{S}}^\top\boldsymbol{\omega} - \tilde{\boldsymbol{\omega}}\tilde{\boldsymbol{S}}\boldsymbol{V} - \tilde{\boldsymbol{\omega}}\boldsymbol{J}'\boldsymbol{\omega} - \frac{1}{m'}\tilde{\boldsymbol{S}}\boldsymbol{F}' + \boldsymbol{M}_f'\right) \tag{37}$$

$$\boldsymbol{g}_2'(\boldsymbol{x}) = \left(\frac{1}{m'}\tilde{\boldsymbol{S}}\tilde{\boldsymbol{S}} + \boldsymbol{J}'\right)^{-1}\boldsymbol{B}_u' \tag{38}$$

where V denotes the airspeed, $\tilde{\boldsymbol{\omega}}$ represents the skew-symmetric matrix of $\boldsymbol{\omega}$, m' denotes the mass for damaged aircraft, $\boldsymbol{J}'$ represents the modeled inertia matrix for damaged aircraft, and $\boldsymbol{F}'$ denotes new total force vector after faults. Denote the distance vector from origin center of mass O to the new c.m. location O' as $\boldsymbol{r}_{OO'} = [r_{\Delta x}, r_{\Delta y}, r_{\Delta z}]^\top$. $\tilde{\boldsymbol{S}}$ denotes the skew-symmetric matrix of the corresponding vector $[m'r_{\Delta x}, m'r_{\Delta y}, m'r_{\Delta z}]^\top$. It is nonzero when using the non-center of mass approach, which leads to coupled translational and rotational motions. After structural damage, control reversal, and/or actuator fault occurs, the $\boldsymbol{B}_u'\boldsymbol{u} \in \mathbb{R}^{3\times 1}$ term represents the moment vector generated by control surfaces, while the $\boldsymbol{M}_f' \in \mathbb{R}^{3\times 1}$ term represents the moment vector that is not related to control surface deflections.

For the system given in Eq. (36), the vector relative degree is $\boldsymbol{\rho} = [2, 2, 2]^\top$. Therefore, we obtain

$$\begin{aligned}\boldsymbol{y}^{(\boldsymbol{2})} = {} & \frac{\partial[\boldsymbol{f}_1(\boldsymbol{x}_1) + \boldsymbol{g}_1(\boldsymbol{x}_1)\boldsymbol{x}_2]}{\partial\boldsymbol{x}_1}(\boldsymbol{f}_1(\boldsymbol{x}_1) + \boldsymbol{g}_1(\boldsymbol{x}_1)\boldsymbol{x}_2) \\ & + \boldsymbol{g}_1(\boldsymbol{x}_1)((1-\kappa)\boldsymbol{f}_2(\boldsymbol{x}) + \kappa\boldsymbol{f}_2'(\boldsymbol{x}) + (1-\kappa)\boldsymbol{g}_2(\boldsymbol{x})\boldsymbol{u} + \kappa\boldsymbol{g}_2'(\boldsymbol{x})\boldsymbol{u})\end{aligned} \tag{39}$$

which further leads to

$$\boldsymbol{\mathcal{B}}(\boldsymbol{x}, \kappa) = \boldsymbol{g}_1(\boldsymbol{x}_1)\big((1-\kappa)\boldsymbol{g}_2(\boldsymbol{x}) + \kappa\boldsymbol{g}_2'(\boldsymbol{x})\big) \tag{40}$$

The A-INDI-SMC method in Eq. (21) is applied for the system in Eq. (36) as

$$\Delta\boldsymbol{u}_{a-i-s}(k) = \hat{\boldsymbol{\Lambda}}(k)(\hat{\boldsymbol{\mathcal{B}}}_0(k))^{-1}\Big(\boldsymbol{v}_c(k) + \boldsymbol{v}_s(k) - \hat{\boldsymbol{y}}_0^{(\boldsymbol{2})}(k)\Big) \tag{41}$$

where the nominal control effective matrix is $\hat{\boldsymbol{\mathcal{B}}}_0(k) = \boldsymbol{g}_1(\boldsymbol{x})\boldsymbol{g}_2(\boldsymbol{x})|_0$. For an aircraft with actuator fault and structural damage, it is reasonable to assume that $\tilde{\boldsymbol{\Delta}}_s$ is bounded [21]. Therefore, using Theorem 1, for faults scenarios that satisfy Assumption 2 (for the system modeled as Eq. (36), this is equivalent to $\|(\kappa\boldsymbol{g}_1(\boldsymbol{x}_1)(\boldsymbol{g}_2'(\boldsymbol{x}) - \boldsymbol{g}_2(\boldsymbol{x}))|_0)(\boldsymbol{g}_1(\boldsymbol{x})\boldsymbol{g}_2(\boldsymbol{x})|_0)^{-1}\| < 1$), and the newly proposed A-INDI-SMC guarantees stable fault-tolerant tracking.

B. Numerical Simulations

The designed fault-tolerant flight control in Sec. III will be numerically evaluated on a public model of F-16. Actuators are modeled as second-order linear systems with rate and position limits (parameters

from Table 2 of Ref. [21]). The fault cases considered in this section include the effectiveness loss and jamming of rudder, aileron, elevator, structural damage, as well as control reversal. The influences of actuator faults and structural damage are modeled using the methods in [21].

The simulated fault scenarios are as follows. The actuator faults happen at $t = 2$ s: the aileron lost 30% of its effectiveness; the elevator lost 50% of its the effectiveness; the rudder lost 40% of its effectiveness. Moreover, at $t = 2$ s, the right aileron runs away and get jammed at 15.05°. The solid OFC fault is also added to the left elevator. Apart from these actuator faults, structural damage is added from $t = 8$ s. Specifically, the right wing lost 25% of its area; the entire left horizontal stabilator and a half of the vertical tail are also lost. On top of these faults, the actuation sign of all actuators is reversed at $t = 14$ s, and are then reversed again at $t = 24$ s.

The angular acceleration sensor dynamics (containing bias) is modeled as a first-order linear system $G_a(s) = 1.4/0.02s + 1$, using the ideal angular acceleration measurement as the input. In addition, the power spectral density (PSD) height of the angular acceleration measurement noise is set to 10^{-5}. Parametric uncertainties with magnitudes lower than 10% are also added during simulations.

The attitude tracking commands are designed as smoothly combined sigmoid functions. If the reference is not continuous, it is suggested to use command filtering to smoothen the reference. The aircraft is initially trimmed at a steady-level flight condition with airspeed equals 600 ft/s and altitude equals 12,000 ft. The initial states for the aircraft are $\boldsymbol{x}_1 = [0, 0, 0]°$, $\boldsymbol{x}_2 = [0, 0, 0]°/\text{s}$. The sampling interval $h = 0.01$ s. The control parameters are kept invariant as $\boldsymbol{K}_1 = [10, 5]$, $\boldsymbol{K}_2 = [10, 5]$, $\boldsymbol{K}_3 = [5, 2]$, $\boldsymbol{K} = \text{diag}\{\boldsymbol{K}_1, \boldsymbol{K}_2, \boldsymbol{K}_3\}$, $\boldsymbol{S}_1 = [5, 1]$, $\boldsymbol{S}_2 = [5, 1]$, $\boldsymbol{S}_3 = [2, 1]$, $K_{s,1} = 1$, $K_{s,2} = 1$, $K_{s,3} = 0.5$, and $\gamma = 0.25$. Furthermore, we choose $N = 3$ and $\tau_d = 0.07$ s in the FDI algorithm. These gain selections lead to $\bar{\lambda} = 0.98$ in Eq. (32).

Three FTC methods are compared: the INDI control method [22], the INDI-SMC method [21], and the A-INDI-SMC proposed in this Note. The simulation results are shown in Figs. 2–6. The attitude tracking responses are given in Fig. 2. It can be observed that the sensing error, actuator faults, and structural damage can be tolerated by the INDI, INDI-SMC, and A-INDI-SMC methods. However, when control reversal occurs at $t = 14$ s, both INDI and INDI-SMC are unable to stabilize the aircraft, while the newly proposed A-INDI-SMC is able to tolerate all the faults while continuing in executing the tracking task. These phenomena confirm Theorem 1 and Remark 4.

The control inputs are shown in Fig. 3a, from which it can be seen that the actuators are saturated under the control of INDI and INDI-SMC when control reversal occurs. By contrast, the proposed A-INDI-SMC does not suffer from saturation or severe oscillations. The sliding variable responses of INDI-SMC [Eq. (8)] and A-INDI-SMC [Eq. (22)] are illustrated in Fig. 3b. It can be observed that the sliding variables of INDI-SMC become unbounded when control reversal happens. By contrast, even though the sliding variables of A-INDI-SMC shortly leave the sliding surfaces when a fault is encountered, they will converge back to the surfaces in finite time.

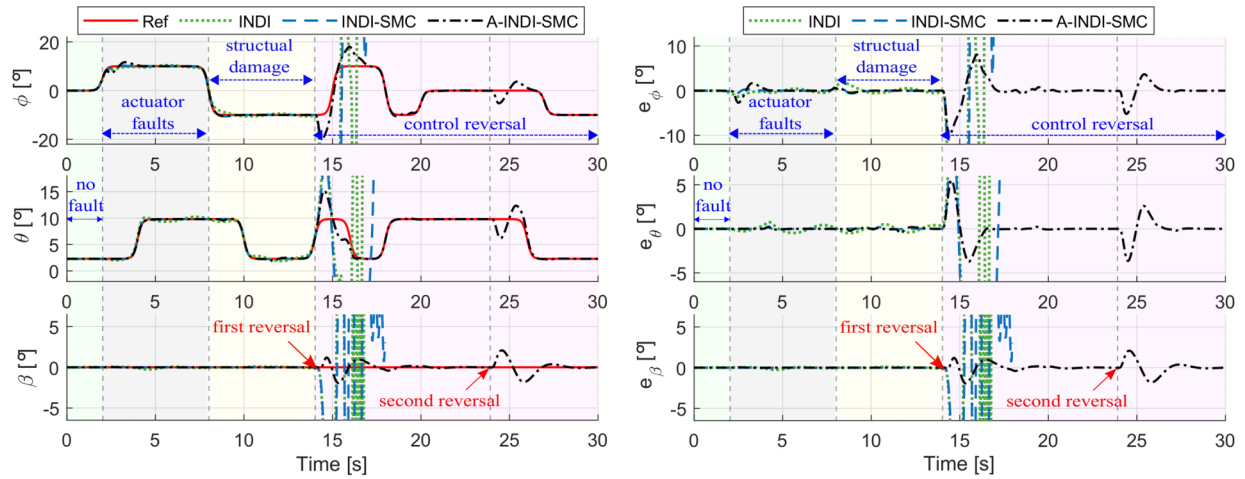

a) Attitude b) Tracking error

Fig. 2 Attitude tracking performance comparisons of INDI, INDI-SMC, and A-INDI-SMC.

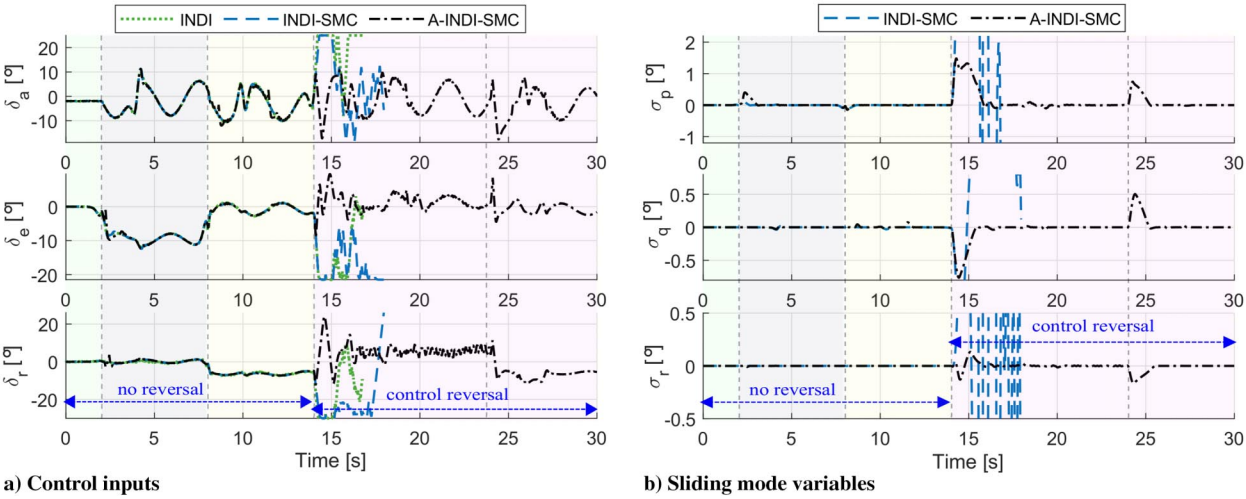

a) Control inputs b) Sliding mode variables

Fig. 3 Control inputs and sliding mode variable responses.

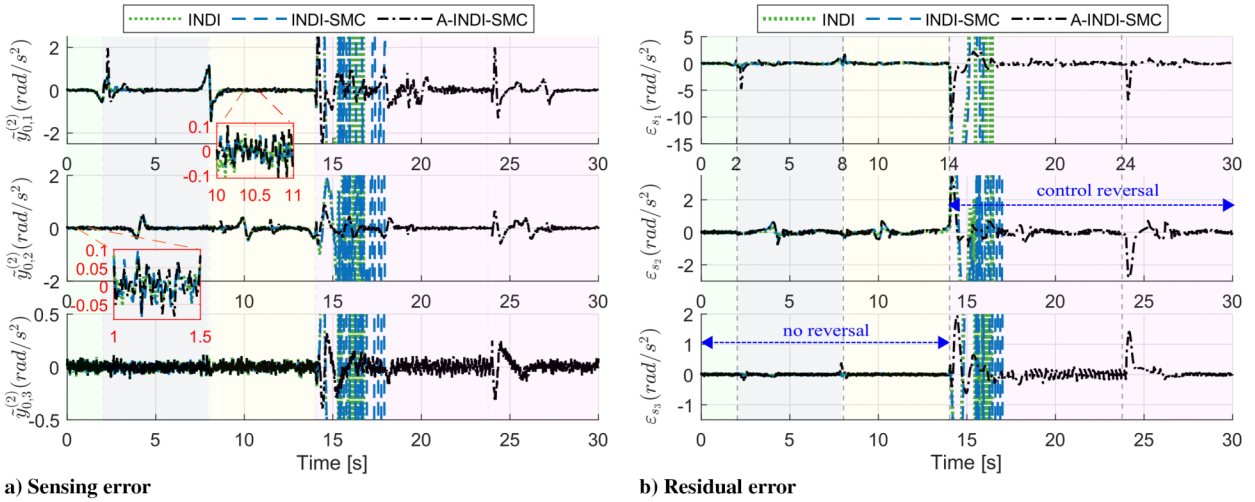

a) Sensing error b) Residual error

Fig. 4 Sensing error and the residual error.

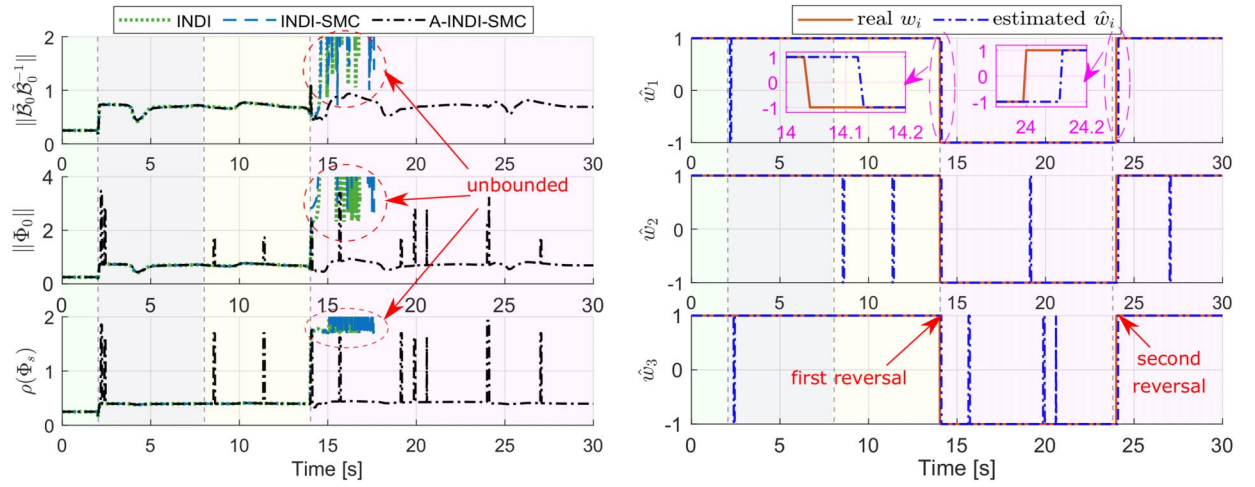

a) Control effectiveness matrix uncertainty b) FDI results

Fig. 5 Responses of control effectiveness uncertainty and the FDI unit identification results.

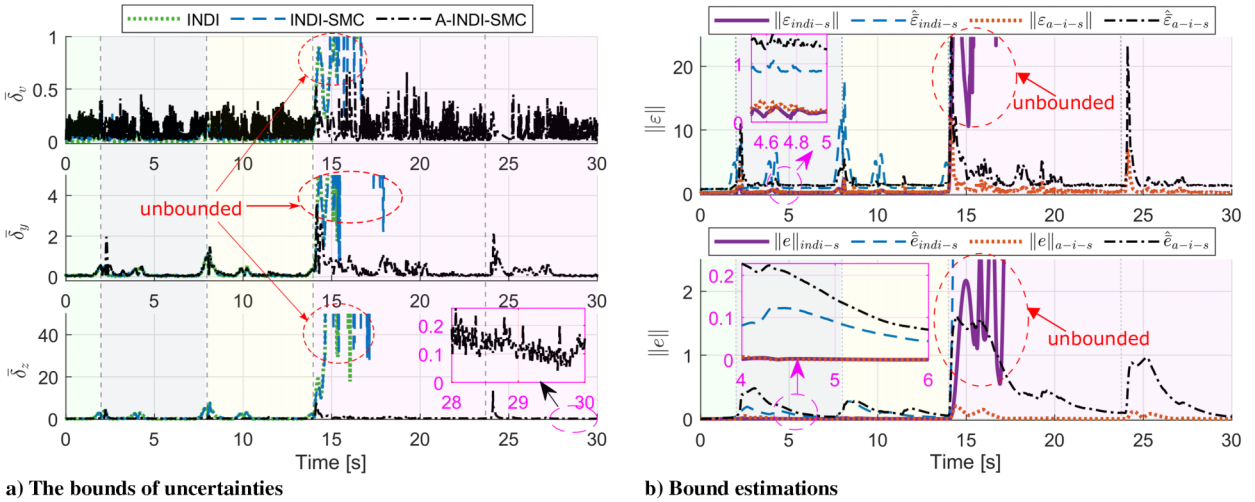

a) The bounds of uncertainties b) Bound estimations

Fig. 6 The bounds of uncertainties and the estimated bounds of the residual and tracking errors.

Figure 4a shows the sensing errors (including noise and time-varying biases) added to the angular acceleration measurements. As explained in Sec. IV.B, the time-varying biases are calculated by filtering the ideal angular acceleration measurements. Since after control reversal happens, INDI and INDI-SMC become unstable, their $\tilde{y}_0^{(2)}$ values also become unbounded. The zoomed-in subplots of Fig. 4a show the influences of measurement noise in steady-state phases.

The residual cancellation errors are presented in Fig. 4b. It can be seen that $\boldsymbol{\varepsilon}_{\text{indi}}$ and $\boldsymbol{\varepsilon}_{\text{indi-}s}$ remain bounded when no reversal happens ($\|\boldsymbol{\Phi}_0(\boldsymbol{x})\| \leq \bar{b} < 1$), which confirms Lemma 1. However, after control reversal is encountered, $\boldsymbol{\varepsilon}_{\text{indi}}$ and $\boldsymbol{\varepsilon}_{\text{indi-}s}$ become unbounded, which confirms Remark 1 and Remark 4. On the contrary, with the help of incremental FE, A-INDI-SMC is able to guarantee an unbounded $\boldsymbol{\varepsilon}_{a-i-s}$, verifying the discussions in Remark 4. This boundedness is of crucial importance for maintaining stable tracking (Fig. 2) in faulty scenario.

The control effectiveness matrix uncertainties $\|\tilde{\boldsymbol{\mathcal{B}}}_0\hat{\boldsymbol{\mathcal{B}}}_0^{-1}\|$, $\|\boldsymbol{\Phi}_0\|$, and $\rho(\boldsymbol{\Phi}_s)$ are illustrated in Fig. 5a. Assumption 2, $\|\tilde{\boldsymbol{\mathcal{B}}}_0(\boldsymbol{x})\hat{\boldsymbol{\mathcal{B}}}_0^{-1}(\boldsymbol{x})\| \leq \bar{b} < 1$, is satisfied. Moreover, it can be seen that the condition $\|\boldsymbol{\Phi}_0(\boldsymbol{x})\| \leq \bar{b} < 1$ is violated using INDI and INDI-SMC after control reversal occurs as discussed in Remark 1. The fault detection results in Fig. 5b show that by using A-INDI-SMC, the control reversals are identified within 0.2 s. The spikes in $\hat{w}_i$ and $\rho(\boldsymbol{\Phi}_s)$ are mainly caused by multisource faults. Shortly after a fault is encountered or when the tracking commands change rapidly, the inequality in Eq. (18) can be violated in short intervals. Nevertheless, Fig. 5b shows that these intervals are much shorter than the intervals where the control directions are correctly identified. Therefore, according to Remark 5, the system using A-INDI-SMC remains stable, which is verified by Fig. 2.

To analyze the impacts of various sources of uncertainty on the ultimate bound of the residual and tracking errors, the trajectories of $\bar{\delta}_y(k) = \|\tilde{\boldsymbol{y}}_0(k)\|$, $\bar{\delta}_z(k) = \|\boldsymbol{y}^{(\rho)}(k) - \hat{\boldsymbol{y}}_0^{(\rho)}(k) - \boldsymbol{\mathcal{B}}_0(k)\Delta\boldsymbol{u}(k)\|$, $\bar{\delta}_v(k) = \|\boldsymbol{v}_c(k) + \boldsymbol{v}_s(k) - \boldsymbol{v}_c(k-1) - \boldsymbol{v}_s(k-1)\|$, and $\bar{\delta}_\sigma(k) = \|\Delta\boldsymbol{\sigma}(k)\|$ are plotted. The estimated upper bounds of the residual cancellation error of INDI-SMC and A-INDI-SMC are calculated using Eq. (28) as $\hat{\bar{\boldsymbol{\varepsilon}}}(k) = \bar{b}\hat{\bar{\boldsymbol{\varepsilon}}}(k-1) + \bar{b}\bar{\delta}_v(k-1) + \hat{\bar{\delta}}_y(k-1) + \hat{\bar{\delta}}_z(k-1)$. Moreover, their tracking error upper bounds are estimated using Eq. (31) as $\hat{\bar{\boldsymbol{e}}}(k) = \bar{\lambda}\,\hat{\bar{\boldsymbol{e}}}(k-1) + \bar{\delta}_\sigma(k-1)$. The terms $\hat{\bar{\delta}}_i$, $i = y, z$, are the known approximations of the upper bounds $\bar{\delta}_i$, $i = y, z$, with $\hat{\bar{\delta}}_i \geq \bar{\delta}_i$.

Figure 6 shows the bounds of uncertainties and the estimated bounds of residual and tracking errors. It can be seen that the variations of $\bar{\delta}_v$, $\bar{\delta}_y$, and $\bar{\delta}_z$ are induced by faults and command variations. After a perturbation occurs, $\bar{\delta}_z$ gradually converges to a small bound around zero. Moreover, when using INDI and INDI-SMC, these state-related uncertainties become unbounded after control reversal happens. Comparing the relative magnitudes of the uncertainties, Fig. 6a shows that $\bar{\delta}_z$ has the highest magnitude throughout the time history, which is followed by $\bar{\delta}_y$. As discussed in Sec. III.C, under high sampling frequency, the variations of virtual control have limited impacts on the closed-loop behavior, which is verified by the small magnitude of $\bar{\delta}_v$. Figure 6b verifies that the real $\|\boldsymbol{e}\|$ and $\|\boldsymbol{e}\|$ are indeed always smaller than their estimated bound. Regarding the ultimate bounds of $\boldsymbol{\varepsilon}_{a-i-s}$ and $\boldsymbol{e}$, they can be estimated by Eqs. (29) and (33) as $\|\boldsymbol{\varepsilon}_{a-i-s}\| \leq 1.3425$ rad/s^2 and $\|\boldsymbol{e}\| \leq 0.0180$ rad. These values are very close and slightly larger than the true ultimate bounds shown in Figs. 2b and 6b: $\|\boldsymbol{\varepsilon}_{a-i-s}\| \leq 0.2210$ rad/s^2 and $\|\boldsymbol{e}\| \leq 0.0101$ rad. These results confirm the ultimate bound estimation expressions in Eqs. (29) and (33).

In summary, Figs. 2–6 verify that the proposed A-INDI-SMC can actively resist parametric model uncertainties, actuator faults, structural damage, and control reversal, while the tracking error $\boldsymbol{e}$ and the uncertainty $\boldsymbol{\varepsilon}$ all become unbounded if control reversal occurs when INDI and INDI-SMC in the literature are applied.

V. Conclusions

This Note aims for designing a nonlinear control method that can actively tolerate sudden in-flight control reversal, parametric model uncertainties, sensing errors, actuator faults, and structural damage. The promising incremental sliding mode control (INDI-SMC) method, which is a hybridization between nonlinear incremental control and sliding mode control, is first analyzed. Lyapunov-based stability and robustness analysis exposes that there exists a critical sufficient condition for ensuring the boundedness of the residual error and the stability of the closed-loop system. However, even though this sufficient condition is normally satisfied in moderate damage cases, some severe faults, including control reversal, can violate it, leading to instability.

In view of this critical limitation, this Note proposes an active incremental sliding mode control approach, denoted as A-INDI-SMC. An FDI unit is designed that can promptly reconstruct control sign switches in the presence of multisource faults, sensing bias and noise, and model uncertainties. It is also shown that this FDI unit is free from Zeno behavior. Lyapunov-based stability and robustness analysis proves that the proposed A-INDI-SMC can guarantee system stability even in the presence of control reversal by virtue of the FDI unit. Moreover, previously ignored sensing imperfections, including sensor lagging dynamics, bias, and noise, are considered in the analysis. Furthermore, explicit and quantifiable expressions for the ultimate bounds of the tracking error and residual error as a function of the sampling frequency and perturbation bounds are derived. This allows selecting the sampling frequency and control parameters based on performance requirements.

The theoretical outcomes are verified by an aircraft command tracking problem with sudden in-flight control reversal, parametric model uncertainties, sensing errors, actuator faults, and structural damage. Simulation results show that although the INDI and the INDI-SMC can passively tolerate some actuator faults and structural damage, they both become unstable when control reversal occurs. By contrast, the proposed A-INDI-SMC method can actively and simultaneously resist all the simulated sudden faults. Its sliding variables also converge to zero in finite time after faults happen. Moreover, the proposed incremental FDI unit is able to reconstruct the switched control sign within 0.2 s. Furthermore, the theoretical ultimate bound expressions for the tracking error and residual error, explicitly including sampling frequency, are also verified by numerical simulations.

Acknowledgment

This work was supported by the National Natural Science Foundation of China under Grant 62003252.

References

[1] Lewis, J. A., and Johnson, E. N., "Gain Switching Control Law for Dynamic Inversion Based Adaptive Control with Unknown Sign of Control Effectiveness," *AIAA SciTech 2021 Forum*, AIAA Paper 2021-0529, 2021. https://doi.org/10.2514/6.2021-0529

[2] Rose, J. B. R., and Jinu, G., "Influence of Aeroelastic Control Reversal Problem in the Airplane Lateral Stability Modes," *Proceedings of the Institution of Mechanical Engineers, Part G: Journal of Aerospace Engineering*, Vol. 229, No. 3, 2015, pp. 517–533. https://doi.org/10.1177/0954410014537241

[3] "Aircraft Accident Report: Uncontrolled Descent and Collision with Terrain, United Airlines Flight 585, Boeing 737-200, N999UA, 4 Miles South of Colorado Springs Municipal Airport, Colorado Springs, Colorado, March 3, 1991," National Transportation Safety Board, Washington, D.C., March 2001, pp. 12–55, https://www.ebay.com/itm/.

[4] Dismukes, R. K., Berman, B. A., and Loukopoulos, L., *The Limits of Expertise: Rethinking Pilot Error and the Causes of Airline Accidents*, Routledge, London, 2007, Chap. 2. https://doi.org/10.4324/9781315238654

[5] Day, R. E., *Coupling Dynamics in Aircraft: a Historical Perspective*, Vol. 532, Office of Management, Scientific and Technical Information Program, NASA, Washington, D.C., 1997, pp. 2–4.

[6] Ackerman, K. A., Xargay, E., Choe, R., Hovakimyan, N., Cotting, M. C., Jeffrey, R. B., Blackstun, M. P., Fulkerson, T. P., Lau, T. R., and Stephens, S. S., "Evaluation of an L 1 Adaptive Flight Control Law on Calspan's Variable-Stability Learjet," *Journal of Guidance, Control, and Dynamics*, Vol. 40, No. 4, 2017, pp. 1051–1060. https://doi.org/10.2514/1.G001730

[7] Hamayun, M. T., Edwards, C., and Alwi, H., "Design and Analysis of an Integral Sliding Mode Fault-Tolerant Control Scheme," *IEEE Transactions on Automatic Control*, Vol. 57, No. 7, 2011, pp. 1783–1789. https://doi.org/10.1109/TAC.2011.2180090

[8] Nussbaum, R. D., "Some Remarks on a Conjecture in Parameter Adaptive Control," *Systems and Control Letters*, Vol. 3, No. 5, 1983,

pp. 243–246.
https://doi.org/10.1016/0167-6911(83)90021-X
[9] Kaloust, J., and Qu, Z., "Continuous Robust Control Design for Nonlinear Uncertain Systems Without a Priori Knowledge of Control Direction," *IEEE Transactions on Automatic Control*, Vol. 40, No. 2, 1995, pp. 276–282.
https://doi.org/10.1109/9.341792
[10] Chen, Z., "Nussbaum Functions in Adaptive Control with Time-Varying Unknown Control Coefficients," *Automatica*, Vol. 102, Dec. 2019, pp. 72–79.
https://doi.org/10.1016/j.automatica.2018.12.035
[11] Wang, C., Wen, C., and Guo, L., "Multivariable Adaptive Control with Unknown Signs of the High-Frequency Gain Matrix Using Novel Nussbaum Functions," *Automatica*, Vol. 111, Jan. 2020, Paper 108618.
https://doi.org/10.1016/j.automatica.2019.108618
[12] Abbaspour, A., Mokhtari, S., Sargolzaei, A., and Yen, K. K., "A Survey on Active Fault-Tolerant Control Systems," *Electronics*, Vol. 9, No. 9, 2020, p. 1513.
https://doi.org/10.3390/electronics9091513
[13] Zhu, S., Wang, D., Shen, Q., and Poh, E. K., "Satellite Attitude Stabilization Control with Actuator Faults," *Journal of Guidance, Control, and Dynamics*, Vol. 40, No. 5, 2017, pp. 1304–1313.
https://doi.org/10.2514/1.G001922
[14] Cristofaro, A., and Johansen, T. A., "Fault Tolerant Control Allocation Using Unknown Input Observers," *Automatica*, Vol. 50, No. 7, 2014, pp. 1891–1897.
https://doi.org/10.1016/j.automatica.2014.05.007
[15] Chang, J., Cieslak, J., Guo, Z., and Henry, D., "On the Synthesis of a Sliding-Mode-Observer-Based Adaptive Fault-Tolerant Flight Control Scheme," *ISA Transactions*, Vol. 111, May 2021, pp. 8–23.
https://doi.org/10.1016/j.isatra.2020.10.061
[16] Lu, P., Van Eykeren, L., Van Kampen, E., De Visser, C., and Chu, Q., "Adaptive Three-Step Kalman Filter for Air Data Sensor Fault Detection and Diagnosis," *Journal of Guidance, Control, and Dynamics*, Vol. 39, No. 3, 2016, pp. 590–604.
https://doi.org/10.2514/1.G001313
[17] Feng, L., Chai, Y., Xu, S., and Yang, Z., "Observer-Based Fault Estimators Using Iterative Learning Scheme for Nonlinear Time-Delay Systems with Intermittent Faults," *International Journal of Robust and Nonlinear Control*, Vol. 27, No. 17, 2017, pp. 3412–3432.
https://doi.org/10.1002/rnc.3747
[18] Zhu, J.-W., and Yang, G.-H., "Robust Distributed Fault Estimation for a Network of Dynamical Systems," *IEEE Transactions on Control of Network Systems*, Vol. 5, No. 1, 2016, pp. 14–22.
https://doi.org/10.1109/TCNS.2016.2567223
[19] Ma, Y., Tao, G., Jiang, B., and Cheng, Y., "Multiple-Model Adaptive Control for Spacecraft Under Sign Errors in Actuator Response," *Journal of Guidance, Control, and Dynamics*, Vol. 39, No. 3, 2016, pp. 628–641.
https://doi.org/10.2514/1.G001352
[20] Ma, Y., Ren, H., Tao, G., and Jiang, B., "Adaptive Compensation for Actuation Sign Faults of Flexible Spacecraft," *IEEE Transactions on Aerospace and Electronic Systems*, Vol. 57, No. 2, 2021, pp. 1288–1300.
https://doi.org/10.1109/TAES.2020.3040518
[21] Wang, X., van Kampen, E.-J., Chu, Q., and Lu, P., "Incremental Sliding-Mode Fault-Tolerant Flight Control," *Journal of Guidance, Control, and Dynamics*, Vol. 42, No. 2, 2019, pp. 244–259.
https://doi.org/10.2514/1.G003497
[22] Smeur, E. J., Chu, Q., and de Croon, G. C., "Adaptive Incremental Nonlinear Dynamic Inversion for Attitude Control of Micro Air Vehicles," *Journal of Guidance, Control, and Dynamics*, Vol. 39, No. 3, 2016, pp. 450–461.
https://doi.org/10.2514/1.G001490
[23] Wang, X., Van Kampen, E.-J., Chu, Q., and Lu, P., "Stability Analysis for Incremental Nonlinear Dynamic Inversion Control," *Journal of Guidance, Control, and Dynamics*, Vol. 42, No. 5, 2019, pp. 1116–1129.
https://doi.org/10.2514/1.G003791
[24] Nabi, H., Lombaerts, T., Zhang, Y., van Kampen, E., Chu, Q., and de Visser, C. C., "Effects of Structural Failure on the Safe Flight Envelope of Aircraft," *Journal of Guidance, Control, and Dynamics*, Vol. 41, No. 6, 2018, pp. 1257–1275.
https://doi.org/10.2514/1.G003184
[25] Yu, Z., and Crassidis, J. L., "Accelerometer Bias Calibration Using Attitude and Angular Velocity Information," *Journal of Guidance, Control, and Dynamics*, Vol. 39, No. 4, 2016, pp. 741–753.
https://doi.org/10.2514/1.G001437
[26] Kim, S., Tadiparthi, V., and Bhattacharya, R., "Computationally Efficient Attitude Estimation with Extended H 2 Filtering," *Journal of Guidance, Control, and Dynamics*, Vol. 44, No. 2, 2021, pp. 418–427.
https://doi.org/10.2514/1.G005140
[27] Li, Y., Liu, X., Lu, P., He, Q., Ming, R., and Zhang, W., "Angular Acceleration Estimation-Based Incremental Nonlinear Dynamic Inversion for Robust Flight Control," *Control Engineering Practice*, Vol. 117, Dec. 2021, Paper 104938.
https://doi.org/10.1016/j.conengprac.2021.104938
[28] Bhardwaj, P., Akkinapalli, V. S., Zhang, J., Saboo, S., and Holzapfel, F., "Adaptive Augmentation of Incremental Nonlinear Dynamic Inversion Controller for an Extended f-16 Model," *AIAA Scitech 2019 Forum*, AIAA Paper 2019-1923, 2019.
https://doi.org/10.2514/6.2019-1923
[29] Cieslak, J., Efimov, D., and Henry, D., "Transient Management of a Supervisory Fault-Tolerant Control Scheme Based on Dwell-Time Conditions," *International Journal of Adaptive Control and Signal Processing*, Vol. 29, No. 1, 2015, pp. 123–142.
https://doi.org/10.1002/acs.2465
[30] Su, W.-C., Drakunov, S., and Ozguner, U., "An O (T^2) Boundary Layer in Sliding Mode for Sampled-Data Systems," *IEEE Transactions on Automatic Control*, Vol. 45, No. 12, Dec. 2000, pp. 2427–2432.
https://doi.org/10.1109/9.895588
[31] Jeon, B.-J., Seo, M.-G., Shin, H.-S., and Tsourdos, A., "Understandings of Classical and Incremental Backstepping Controllers with Model Uncertainties," *IEEE Transactions on Aerospace and Electronic Systems*, Vol. 56, No. 4, 2019, pp. 2628–2641.
https://doi.org/10.1109/TAES.2019.2952631